



HAL
open science

Buoyancy and localizing properties of continental mantle lithosphere: Insights from thermomechanical models of the eastern Gulf of Aden

Louise Watremez, Evgenii E.B. Burov, Elia d'Acremont, Sylvie Leroy, Benjamin Huet, Laetitia Le Pourhiet, Nicolas Bellahsen

► To cite this version:

Louise Watremez, Evgenii E.B. Burov, Elia d'Acremont, Sylvie Leroy, Benjamin Huet, et al.. Buoyancy and localizing properties of continental mantle lithosphere: Insights from thermomechanical models of the eastern Gulf of Aden. *Geochemistry, Geophysics, Geosystems*, 2013, 14 (8), pp.2800-2817. 10.1002/ggge.20179 . hal-00826216

HAL Id: hal-00826216

<https://hal.science/hal-00826216v1>

Submitted on 27 May 2013

HAL is a multi-disciplinary open access archive for the deposit and dissemination of scientific research documents, whether they are published or not. The documents may come from teaching and research institutions in France or abroad, or from public or private research centers.

L'archive ouverte pluridisciplinaire **HAL**, est destinée au dépôt et à la diffusion de documents scientifiques de niveau recherche, publiés ou non, émanant des établissements d'enseignement et de recherche français ou étrangers, des laboratoires publics ou privés.

1 Buoyancy and localizing properties of continental
2 mantle lithosphere: Insights from thermomechanical
3 models of the eastern Gulf of Aden

L. Watremez,^{1,2,3} E. Burov,^{2,3} E. d'Acremont,^{2,3} S. Leroy,^{2,3} B. Huet,⁴ L. Le

Pourhiet,^{2,3} and N. Bellahsen^{2,3}

Corresponding author: L. Watremez, Department of Oceanography, Dalhousie University, Halifax, NS B3H 4R2, Canada. (louise.watremez@dal.ca)

¹Department of Oceanography, Dalhousie University, Halifax, NS, Canada

²ISTeP, UPMC University Paris 06 - UMR 7193, Paris, France

³ISTeP, CNRS UMR 7193, Paris, France

⁴Department for Geodynamics and Sedimentology, University of Vienna, A-1090 Vienna, Austria

4 **Abstract.** Physical properties of the mantle lithosphere have a strong
5 influence on the rifting processes and rifted structures. In particular, in con-
6 text of rifting, two of these properties have been overlooked: (1) Mohr-Coulomb
7 plasticity (localizing pressure-dependent) may not be valid at mantle depths
8 as opposed to non-localizing pressure-independent plasticity (hereafter, per-
9 fect plasticity), and (2) lithosphere buoyancy can vary, depending on the petro-
10 logical composition of the mantle. Focussing on the Arabian plate, we show
11 that the lithosphere may be negatively buoyant. We use thermomechanical
12 modeling to investigate the importance of mantle rheology and composition
13 on the formation of a passive margin, ocean-continent transition (OCT) and
14 oceanic basin. We compare the results of this parametric study to observa-
15 tions in the eastern Gulf of Aden (heat-flow, refraction seismics and topog-
16 raphy) and show that (1) mantle lithosphere rheology controls the margin
17 geometry and timing of the rifting; (2) lithosphere buoyancy has a large im-
18 pact on the seafloor depth and the timing of partial melting; and (3) a per-
19 fectly plastic mantle lithosphere 20 kg m^{-3} denser than the asthenosphere
20 best fits with observed elevation in the Gulf of Aden. Finally, thermomechan-
21 ical models suggest that partial melting can occur in the mantle during the
22 Arabian crustal break-up. We postulate that the produced melt could then
23 infiltrate through the remnant continental mantle lithosphere, reach the sur-
24 face and generate oceanic crust. This is in agreement with the observed nar-
25 row OCT composed of exhumed continental mantle intruded by volcanic rocks
26 in the eastern Gulf of Aden.

1. Introduction

27 Whether or not a large amount of magmatic activity occurs during rifting has led to
28 two separate classes of rifted passive margins: volcanic or non-volcanic margins. Volcanic
29 margins are commonly associated with high thermal anomalies in the mantle, which are
30 often due to mantle plumes like the Afar Plume in the western Gulf of Aden [e.g. *Courtillot*
31 *et al.*, 1999] or the Icelandic Plume in Greenland and Norway [e.g. *Eldholm and Grue*,
32 1994]. These are characterized by basalt flows (seaward dipping reflectors), volcanoes, and
33 mafic underplating produced during the rifting process [e.g. *Mutter et al.*, 1982; *White*
34 *and McKenzie*, 1989; *Geoffroy*, 2005]. These margins present a sharp ocean-continent
35 boundary or a very narrow ocean continent transition zone [OCT, e.g. *Bauer et al.*, 2000;
36 *Mjelde et al.*, 2007].

37 Non-volcanic rifted margins are usually compared to the Iberia margin and are char-
38 acterized by (1) tectonized features (tilted blocks) and a well identified transitional zone
39 between the continental crust and the oceanic crust, the OCT [e.g. *Whitmarsh et al.*, 1991;
40 *Louden et al.*, 1997; *Lavier and Manatschal*, 2006], or (2) a wide zone of hyper-extended
41 crust [e.g. *Contrucci et al.*, 2004; *Unternehr et al.*, 2010]. Non-volcanic margins actually
42 contain a limited amount of magmatism and there is now a general agreement on de-
43 scribing them as magma-poor margin. The nature of the OCT varies along magma-poor
44 margins [e.g. *Leroy et al.*, 2010a; *Gerlings et al.*, 2011]. It is usually either made of (1) a
45 Zone of Exhumed Continental Mantle [Z.E.C.M., e.g. *Manatschal*, 2004], (2) deeper man-
46 tle serpentized by percolation of the seawater through the sediments and faulted crust
47 [e.g. *Boillot et al.*, 1987; *Pérez-Gussinyé and Reston*, 2001], or (3) highly tectonized oceanic

48 crust formed by ultra-slow spreading [e.g. *Srivastava and Roest*, 1995; *Sibuet et al.*, 2007].
49 Another type of magma-poor margin, like the Angolan margin, shows hyper-extended
50 continental crust and evidence of shallow sediments deposition ('sag' basins) during the
51 late phase of rifting [e.g. *Moulin et al.*, 2005].

52 The factors that control the amount of melt produced at magma-poor margins, either by
53 decompressional melting during crustal thinning [e.g. *Minshull*, 2002] or post-rift thermal
54 anomaly [e.g. *Lucazeau et al.*, 2009], are yet to be understood. Especially, it is still not
55 always clear how the properties of the mantle lithosphere affect the rift evolution and the
56 production of melt, i.e. the nature – volcanic or not – of the margin.

57 To answer these types of questions, several studies have shown that comparing me-
58 chanical models of rifted margin formation to data and field observations is an effec-
59 tive approach [e.g. *Brun and Beslier*, 1996; *Lavier and Manatschal*, 2006; *Huismans and*
60 *Beaumont*, 2011]. In particular, *Huismans and Beaumont* [2011] show the importance
61 of a viscous lower crust on the necking of the mantle lithosphere and the geometry of
62 Angolan-type magma-poor margins. The eastern Gulf of Aden has been chosen to tackle
63 the problem of Iberia-type magma-poor margin. Indeed, (1) it is well documented, (2)
64 the conjugate passive margins are known as magma-poor and the width and nature of
65 the OCT vary along the margin [presence of magmatism where the OCT is narrow and
66 exhumed mantle where the OCT is wider, *Leroy et al.*, 2010a], and (3) the oceanic basin
67 is young (oceanic accretion began at least 17.6 Ma ago), so the conjugate margins are
68 easily correlable and numerical modeling of the whole basin is possible.

69 Thermomechanical modeling has been widely used to study the mechanisms of litho-
70 sphere extension and the parameters governing the geometry of rifted structures (e.g.

71 influence of the extension rate, *Bassi, 1995; Van Wijk and Cloetingh, 2002; Huismans and*
72 *Beaumont, 2003; Burov, 2007*; or of the thermal structure of the lithosphere, *Chéry et al.,*
73 *1989*). However, beyond the thermal state and ductile strength of the lithosphere, the
74 effects of (1) plastic behaviour of the mantle lithosphere and (2) buoyancy of the litho-
75 sphere with respect to the underlying asthenosphere, on the structure of passive margins,
76 are not yet well understood. It is indeed questionable whether the standard brittle failure
77 criterion [*Byerlee, 1978*] is applicable to mantle lithosphere [e.g. *Watts and Burov, 2003;*
78 *Bürgmann and Dresen, 2008; Burov, 2011*] or if weaker mechanisms must be included.
79 Similarly, it has become standard to include phase transition and realistic composition
80 in the crust [e.g. *Yamato et al., 2007; Gerya et al., 2008*] to study the dynamic of active
81 margins. However, the effect of petrological composition – and especially the extent of
82 depletion – on the buoyancy of mantle lithosphere during continental extension is rarely
83 taken into account, except to explain post rift subsidence anomalies [*Kaus et al., 2005*].
84 This well might be an important parameter for rifts, which affect continental lithosphere,
85 such as the Rio Grande rift [*Van Wijk et al., 2008*], the Baikal rift [*Petit and Déverchère,*
86 *2006*], or the Gulf of Aden.

87 In this paper, we therefore explore the effect of two overlooked key parameters on rift
88 evolution: (1) the failure criterion acting in mantle lithosphere and (2) the buoyancy of
89 the lithosphere. Then, we compare the results of this parametric study to the heat-flow
90 measurements and wide-angle seismic models at the northern margin, and elevation data
91 across the eastern Gulf of Aden. This allows us to better understand how these two
92 parameters influence the presence of magmatism at the OCT together with the nature
93 and width of the OCT.

2. Geodynamic settings

94 The Arabian plate shows a complex history, with the accretion of terranes in the Neo-
95 Proterozoic [e.g. *Al Hussein*, 2000], the occurrence of the Oman obduction and continental
96 subduction during late Cretaceous [e.g. *Searle*, 1983; *Agard et al.*, 2010] the rifting episode
97 in the Mesozoic [*Bosence*, 1997]. The formation of the Arabian lithosphere is the result of
98 two major tectonic events [*Al Hussein*, 2000]: the Amar collision (640 – 620 Ma) and the
99 Najd rifting (530 – 570 Ma). The ages of the basement rocks of Socotra (southern margin
100 of the eastern Gulf of Aden) are 600 to 860 Ma [U-Pb dating, *Denele et al.*, 2012]. In our
101 models, we therefore consider an approximate age of the Arabian lithosphere of 700 Ma,
102 defining it as a tecton [Neo-Proterozoic lithosphere, e.g. *Griffin et al.*, 2003].

103 The current Gulf of Aden is a young oceanic basin, which separates Arabia from Somalia,
104 accommodating the difference between their plate velocities (Fig. 1). In absolute motion,
105 both plates move to the north. However, the Arabian plate is faster than the Somalian
106 plate [*Vigny et al.*, 2006]. The difference in velocity leads to a present day opening rate of
107 approximately 2 cm yr^{-1} in the eastern Gulf of Aden [e.g. *Fournier et al.*, 2001]. The rifting
108 of the Arabian-Nubian tecton began ~ 34 Ma ago [e.g. *Leroy et al.*, 2012]. Subsequently,
109 seafloor spreading occurred at the latest at 17.6 Ma in the east of the Shukra-el-Sheik
110 Fracture Zone [e.g. *Leroy et al.*, 2004; *d'Acremont et al.*, 2006; *Leroy et al.*, 2012]. A
111 post-rift high thermal regime is observed in the whole Gulf of Aden and is interpreted as
112 being in relation to the Afar hotspot activity [*Lucazeau et al.*, 2009; *Basuyau et al.*, 2010;
113 *Leroy et al.*, 2010b; *Chang and Van der Lee*, 2011].

114 Studies of dynamic topography show that the doming due to the presence of the Afar
115 hotspot does not influence the topography of the eastern Gulf of Aden [e.g. *Lithgow-*

116 *Bertelloni and Silver, 1998*]. Indeed, the eastern Gulf of Aden is roughly 200 km away
117 from the apex of the hotspot. Furthermore, the wavelengths of the structures of the
118 dynamic topography are greater than 4000 km, as they are due to deep mantle sources
119 [e.g. *Hager and Richards, 1989*]. Thus, we do not take the dynamic topography into
120 account in this study.

121 Tomographic studies show that the Arabian-Nubian lithosphere is approximately 250
122 km thick [*Ritsema and van Heijst, 2000; Debayle et al., 2001; Pasyanos and Nyblade,*
123 *2007*]. Receiver functions [*Sandvol et al., 1998; Al Amri, 1999; Pasyanos and Walter,*
124 *2002; Al-Damegh et al., 2005; Tiberi et al., 2007; Al-Hashmi et al., 2011; Al-Lazki et al.,*
125 *2012; Ahmed et al., 2013*] and refraction seismic profiles [*Mooney et al., 1985*] constrain the
126 thickness of the Arabian crust, which varies from 35 km (partly thinned crust, close to the
127 Red Sea and the Gulf of Aden) to 49 km (thickened crust, Oman mountains). We adopt a
128 mean crustal thickness of 44 km for our models, corresponding to the average value of non-
129 thinned and non-thickened Arabian crust. Geophysical studies on the north-eastern Gulf
130 of Aden magma-poor margin show that the OCT is narrow (15 km to 50 km) and presents
131 strong along-margin variations with serpentinization and little volcanism [*Lucazeau et al.,*
132 *2008, 2009, 2010; Autin et al., 2010; Leroy et al., 2010a; Watremez et al., 2011a*].

133 This information will be used both to constrain the initial and boundary conditions
134 of the thermomechanical models presented in section 3 and to compare them with the
135 present structures of the Gulf of Aden. In the parametric study presented here, the aim
136 of the modeling is to better understand the mechanisms of margin formation, such as the
137 north-eastern Gulf of Aden, as well as the nature of their OCT.

3. Parametrization and modeling

3.1. Mantle lithosphere plasticity

138 The Byerlee [1978] failure criterion is commonly used to represent the yield strength
139 behaviour of rocks. Byerlee's law is written in terms of principal stresses. Hence, it
140 may account for pore-fluid pressure or any other deviations from lithostatic pressure.
141 Extrapolating Byerlee's law at pressures corresponding to depths greater than 40 km
142 implies unrealistically high yield strength for the lithosphere (up to several GPa). Thus,
143 it may not be applicable to the mantle lithosphere [e.g. *Watts and Burov, 2003; Précigout*
144 *et al., 2007; Burov, 2011*]. At this confining pressure, other mechanisms may limit the
145 strength of rocks, including compaction bands, grain boundary sliding [GBS, e.g. *Précigout*
146 *et al., 2007*] and Peierls creep [high stress creep for stresses $> 10^3$ MPa, *Kameyama*
147 *et al., 1999*]. All these mechanisms limit the strength of the lithosphere at high deviatoric
148 stresses by reducing the pressure dependence of the strength, and decreasing the ability
149 of the lithosphere to localize strain at high strain-rate (except GBS). Furthermore, field
150 observations of exhumed mantle shear zones show strain localization at all scales and no
151 brittle deformation [see a review in *Précigout et al., 2007; Bürgmann and Dresen, 2008*].
152 In contrast, geophysical imaging of active strike slip faults in the mantle suggests that
153 they are broad (>10 -100 km wide) zones of distributed shearing [*Molnar et al., 1999;*
154 *Little et al., 2002; Sol et al., 2007*]. There is obviously a scale effect in this apparent
155 contradiction.

156 To model the brittle-ductile behaviour of rocks, one can use visco-elasto-plastic rheolo-
157 gies based on Maxwell summation for deviatoric strain-rate ($\dot{\epsilon}^d$):

$$\dot{\epsilon}^d = \dot{\epsilon}_{vis}^d + \dot{\epsilon}_{elas}^d + \dot{\epsilon}_{plas}^d \quad (1)$$

158 The viscous part ($\dot{\epsilon}_{vis}^d$) corresponds to the ductile behaviour of rocks and accounts for
 159 deformation by creep. The elastic strain rate ($\dot{\epsilon}_{elas}^d$) is very small but is needed to model
 160 the path dependence of the rheology. Finally, the brittle part ($\dot{\epsilon}_{plas}^d$) uses a plastic flow
 161 rule to limit the maximal rock strength when a brittle failure criterion is reached. For
 162 Byerlee behaviour, the plastic flow rule follows the *Vermeer* [1990] Mohr-Coulomb plastic
 163 model, but is limited to an incompressible flow (zero dilatation).

164 At high confining pressure, Byerlee's law [1978] shows that maximal brittle strength is
 165 proportional to $0.6 P$, where P is the total pressure. Within our formulation, we model
 166 this experimental law using the cohesion $C_0 = 20$ MPa and the internal friction angle
 167 $\phi = 30^\circ$. If ϕ is not equal to zero, this results in strain localization (shear banding) due to
 168 the apparent strain weakening behaviour [*Vermeer*, 1990; *Le Pourhiet*, 2013]. Mechanisms
 169 such as Peierls [for lithospheric extension, e.g. *Popov and Sobolev*, 2008] and GBS [e.g.
 170 *Précigout et al.*, 2007] creeps are shown to limit rock strength to 400 to 700 MPa [*Burov*,
 171 2011] and to be weakly pressure dependent. Using the creep parameters of *Hirth and*
 172 *Kohlstedt* [2003] and considering the mean strain rate in the rift area of 10^{-14} s^{-1} , a
 173 mantle temperature of 650°C , corresponding to depths of approximately 100 km and an
 174 average grain size of $100 \mu\text{m}$, the value of the GBS yield stress is approximately 400-500
 175 MPa. Thus, we roughly approximated these mechanisms with $C_0 = 450$ MPa and $\phi = 0^\circ$.
 176 As a result, the lithosphere behaves as a perfectly plastic material and no significant
 177 localization, without an additional softening law, is predicted to occur. This mechanism
 178 is also known as "stress limiter" [*van Hunen et al.*, 2002].

179 Thus, while Byerlee's parameters predict a large strength peak at ~ 90 km depth (more
180 than 1 GPa), the maximal strength in the perfectly plastic mantle lithosphere is constant
181 and limited to a much smaller value (in this study, 450 MPa) for the whole depth interval
182 in the mantle lithosphere, up to 100 km depth (Fig. 2).

3.2. Lithosphere buoyancy

183 In order to get direct information on the buoyancy of the Arabian mantle lithosphere,
184 density profiles have been calculated for the chemical compositions of Arabian plate mantle
185 xenoliths available in the literature. These calculations have been carried out using the
186 free energy minimization thermodynamic code PERPLEX07 [Connolly, 2009], together
187 with a recent thermodynamic database and activity models developed for mantle pressure
188 and temperature conditions and compositions [Xu *et al.*, 2008]. Four average compositions
189 of tecton subcontinental mantle lithosphere [Griffin *et al.*, 2009] were also considered as
190 standard compositions for lithospheres having similar age as the Arabian plate. Since the
191 composition of the asthenosphere below the Arabian plate is unknown, we used the fertile
192 Hawaiian pyrolite composition [Wallace and Green, 1991]. This standard is used as a
193 proxy for the density of the asthenosphere influenced by the Afar hot-spot. The buoyancy
194 is calculated as the density difference between asthenosphere and mantle lithosphere:
195 $\rho_{asth} - \rho_{lith}$. The dataset of chemical compositions, the description of the method and the
196 density curves are presented in the Supplementary material.

197 The chemical composition of the xenoliths and the standards are plotted in a Mg# vs.
198 %Al₂O₃ diagram (Fig. 3A). The xenoliths from the Arabian plate are divided into two
199 chemical groups. The depleted group (Iherzolites and harzburgites) plot in the depleted
200 part of the tecton xenoliths (dotted red zone on Fig. 3A). The corresponding compositions

201 are also more depleted than the tecton and asthenosphere standards. The fertile group
202 (clinopyroxenites and websterites) shows greater scatter.

203 The clinopyroxenites and websterites are partly [*Henjes-Kunst et al.*, 1990] or entirely
204 [*Stein et al.*, 1993] interpreted as cumulates formed in Pan-African times. These authors
205 do not explicitly specify the geodynamic context for the formation of these rocks. Com-
206 parison with modern magmatic arcs [e.g. *Saleeby et al.*, 2003] suggests that they formed
207 as cumulates below arcs, which is consistent with the accretion of the Arabian shield
208 during the end of the Pan-African orogeny [*Frisch and Al-Shanti*, 1977; *Hargrove et al.*,
209 2006]. These rocks could also correspond to recycled subducted oceanic crust that has
210 been incorporated into the lithosphere during cooling of the mantle [*Hofmann and White*,
211 1982]. Amounts of recycled oceanic crust in the asthenosphere range mainly between 10%
212 and 20% and reach up to 30% [*Sobolev et al.*, 2007].

213 The calculated depth profiles of buoyancy are presented in Fig. 3B. Chemical variations
214 are directly reflected by the buoyancy. The more depleted is the composition (low %
215 of Al_2O_3 and high Mg#), the greater is the buoyancy. Lherzolites and harzburgites
216 are buoyant or have a slightly negative buoyancy, whereas all clinopyroxenites and the
217 websterites have a very negative buoyancy. Mean buoyancies averaged over the lithosphere
218 are approximately 20 kg m^{-3} for the lherzolite-harzburgite group, -100 kg m^{-3} for the
219 clinopyroxenite-websterite group and 5 kg m^{-3} for the tecton standards.

220 The Arabian plate mantle lithosphere is a mixing of depleted and fertile rocks, both
221 groups having different buoyancies. The buoyancy of the whole lithosphere can therefore
222 be estimated by a weighted average of the buoyancy of these two end-members. In order
223 to take into account the complex history of the Arabian plate, we propose two models

(Fig. 3C). In the first model, the depletion of lherzolites and harzburgites is inherited from partial melting coeval with the formation of the Arabian shield [Stein *et al.*, 1993]. The depleted end-member corresponds to the mean of the lherzolite-harzburgite group. The fertile end-member corresponds to the mean of the clinopyroxenite-websterite group (blue line on 3C). A mantle lithosphere composed of 35% clinopyroxenite-websterite and 65% lherzolite-harzburgite has a negative buoyancy of $\sim 20 \text{ kg m}^{-3}$. In the second model, the depletion is due to Miocene partial melting that postdates the onset of rifting [McGuire, 1988]. The depleted end-member is the mean of the tecton standards and the fertile end-member corresponds to the mean of the clinopyroxenite-websterite group (red line on 3C). 25% clinopyroxenite-websterite is sufficient to explain a negative buoyancy of $\sim 20 \text{ kg m}^{-3}$. A few 10s kg m^{-3} negative buoyancy can therefore be explained by a significant proportion ($\sim 30\%$) of heavy clinopyroxenite and websterite. Using a different asthenosphere composition indicates a difference of $\sim 10 \text{ kg m}^{-3}$. Hence, a reduction of the amount of clinopyroxenite and websterite by 15-25% would induce an average buoyancy of -20 kg m^{-3} . In the parametric study, we apply a $\pm 30 \text{ kg m}^{-3}$ buoyancy in order to test extreme parameters.

3.3. Parametrization and numerical modeling

We use Flamar 12 [an outgrowth of Paravoz, Burov and Yamato, 2008] that is inspired by the FLAC v3 algorithm [Cundall, 1989; Poliakov *et al.*, 1993]. The numerical method has been described in full detail in previous studies [e.g. Burov and Poliakov, 2001; Burov and Cloetingh, 2009; François *et al.*, in press]. This method can handle a free upper surface boundary condition and almost any visco-elasto-plastic rheology. The algorithm explicitly takes into account elastic-brittle-ductile properties of lithosphere and asthenosphere. Due

246 to the explicit nature of this code for elastic compressibility, temperature, gravity and
247 pressure-dependent body forces are computed without the necessity to use assumptions
248 such as potential temperature. The description is limited here to the details that are the
249 most essential for this study.

250 Our model setup is inspired by previous rifting models achieved with the same numerical
251 thermomechanical code [*Burov, 2007, Fig 2*]. The modeling box is 400 km thick and 1200
252 km wide; grid resolution is 4 km in both directions. The properties of each element of
253 the numerical grid (cell) are defined by the density and the thermal and elasto-visco-
254 plastic parameters of its material. We use a density and rheology structure from the
255 lithosphere and asthenosphere derived from *Ranalli [1995]*. All models include a 44 km
256 thick crust with four horizontal rheological layers. The parameters of the reference model
257 are presented in Table 1. Materials in the specific numerical formulation used for the
258 study are elasto-visco-plastic. To avoid activation of Mohr-Coulomb plastic deformation
259 in the asthenosphere [which is unlikely, e.g. *Watts and Burov, 2003*], we assigned high
260 cohesion values to the asthenosphere.

261 The boundary conditions are (1) horizontal extension velocities (V_{ext}) applied at each
262 vertical side of the model, (2) a Winckler pliable basement that simulates the response to
263 lithostatic pressure variations and (3) a free upper surface boundary condition (free stress
264 and free slip conditions in all directions) combined with a moderate diffusion erosion
265 and sedimentation ($k_{eros} = 50 \text{ m}^2 \text{ yr}^{-1}$) and water-column pressure dependent on the
266 surface topography (Fig. 2). The elevation at each point of the free surface is calculated
267 following the model of *Culling [1960]*, which takes into account the effect of erosion and
268 sedimentation.

269 The assumed initial thermal structure is constrained by the radiogenic heat production
270 in the crust, the age the lithosphere and the temperature at the base of the lithosphere.
271 It is noteworthy that, after 600 Ma, the thermal structure of thermally undisturbed litho-
272 sphere reaches a permanent state. Thus, there is no practical difference in the thermal
273 structure of a 600 Ma or, for example, a 2000 Ma old lithosphere [e.g. *Burov and Diament,*
274 1995]. The thermal age in the models is 700 Ma, to be consistent with the real age of the
275 Arabian shield.

276 The main parameters tested in this study are the plastic failure pressure dependence
277 and the buoyancy of the mantle lithosphere.

3.4. Areas of possible partial melting

278 Partial melting is not supposed to have a strong impact on the overall rift evolution
279 of the Eastern Gulf of Aden, as its rifted margins are magma-poor. The lack of a small
280 production of melt at break-up is therefore a non-negligible constraint on the validity of
281 the models. Some codes include partial melting in the modeling, in order to simulate
282 mantle convection [e.g. *ONeill et al., 2006*]. However, for the sake of simplicity, it is
283 not necessary to directly include partial melting calculations. We follow the simplified
284 approach developed by *McKenzie and Bickle* [1988], which consists in calculating the
285 areas where partial melting can occur. We compute the location of these areas at the
286 post-processing stage. The method uses the model-predicted pressure and temperature
287 conditions in the mantle as input, and output a melt fraction. We consider the areas
288 where the melt fraction [defined in *McKenzie and Bickle, 1988*] is between 0 and 1. This
289 post-processing allows us to assess whether melt can be produced during the rifting and
290 to characterize the nature of the OCT in the model.

4. Parametric study

4.1. Influence of mantle lithosphere rheology

291 Figure 4 compares two models with different mantle rheology and highlights the influ-
292 ence of this parameter on rifting evolution and rifted margins formation.

293 As expected from the rheology law, deformation is more diffuse in the perfectly plastic
294 mantle than in a Byerlee’s mantle. Meanwhile, strain localization is also enhanced by the
295 higher strength of a Byerlee’s lithosphere and the imposed velocity boundary condition.
296 This lack of localization results in delaying the break-up of continental crust by 1.5 Myr
297 for the model with the perfectly plastic mantle. As the strain localization is more in-
298 tense in the Mohr-Coulomb mantle lithosphere, deformation propagates faster through
299 the continental crust. Moreover, the strain rate patterns 0.5 Ma before the break-up of
300 the continental crust show an asymmetric deformation in the upper mantle beneath the
301 continental rift for the Mohr-Coulomb model, while the perfectly plastic model remains
302 symmetric (Fig. 4A).

303 Crustal flexure (shape of the continental crust aside the rift) – and hence flexural stresses
304 – at the time of crustal break-up is more intense for the Mohr-Coulomb model than for
305 the perfectly plastic model, contributing to an earlier break-up for the former (Fig. 4A).
306 As can be seen the local extrema of topography coincide in either case, producing close
307 values of flexural wavelength (~ 250 km) and, hence, of elastic thickness (Fig. 4B). The
308 corresponding equivalent flexural thickness estimated using analytical formulae for the
309 flexural parameter [*Turcotte and Schubert, 2002*] is on the order of 40 km. This wavelength
310 is largely controlled by the strongest part of the mantle lithosphere [*Burov and Diament,*
311 *1995*]. The difference in amplitude at rift flanks refers to smaller levels of flexural stress in

312 the crust in case of a less localizing, perfectly-plastic rheology. We observe that no partial
313 melting can occur in the mantle lithosphere for either model, suggesting that continental
314 mantle can be exhumed without production of oceanic crust in either case.

315 In order to compare the models with the present day Gulf of Aden, we compare their
316 geometries and bathymetries 18 Ma after break-up. The geometry of the structures at
317 this moment also shows a slightly stronger flexure for the Mohr-Coulomb model than
318 for the perfectly plastic model, while conjugate margins are still asymmetric (Fig. 4A).
319 The slope of the Moho discontinuity is also steeper for the Mohr-Coulomb model than
320 for the perfectly plastic model, implying a wider distal margin with the perfectly plastic
321 configuration. Moreover, the ridge location shows a strong asymmetry in the Mohr-
322 Coulomb model, contrary to the perfectly plastic model. This can be attributed to the
323 fact that a Mohr-Coulomb mantle localizes the deformation better, allowing for further
324 strain to occur on the fault formed along the margin at the break-up of the continental
325 crust. Comparison of the topography 18 Ma after continental crust break-up provides a
326 similar amplitude of the topography for both models, but the same asymmetry is recovered
327 as the oceanic ridge is highlighted by a deeper zone along the model (Fig. 4B). We also
328 observe the development of this asymmetry on the evolution of the topography (distance
329 versus time, Fig. 4C). Indeed, after continental break-up, the ridge tends to be localized
330 close to the margin during approximately 10-12 Myr for the Mohr-Coulomb model. The
331 ridge remains stable until the fault zone reaches a hardening sufficient to cause a relocation
332 of the ridge. On the contrary, the ridge in the perfectly plastic model is centered from
333 the onset of the formation of the oceanic basin. This difference is due to the fact that
334 the perfectly plastic mantle has a more diffuse deformation mechanism than the Mohr-

335 Coulomb mantle. The model with the perfectly plastic mantle also shows an oceanic
336 ridge that is centered in the same way as observed in the Gulf of Aden, giving additional
337 preference to the perfectly plastic model over the Mohr-Coulomb model.

338 It can be concluded that the choice of the failure criterion in the mantle lithosphere has
339 a significant impact on the extensional deformation in the upper mantle, and indirectly
340 in the continental crust. Compared to the Mohr-Coulomb mantle, the assumption of a
341 perfectly plastic mantle allows for a more diffuse deformation, with the following conse-
342 quences: (1) more extension is needed to break the crust apart, (2) the flexure is more
343 gentle, and (3) the horizontal position of the oceanic ridge, as observed in the Gulf of
344 Aden, is more consistent with observation. However, oceanic basins predicted by both
345 models are deeper than the observed topography profiles across the Gulf of Aden. Hence,
346 additional factors such as mantle density should be explored to explain the shallowness
347 of the oceanic basin of the Gulf of Aden.

4.2. Influence of lithosphere buoyancy

348 The three model-setups are identical to the Mohr-Coulomb setup previously presented
349 (Table 1), except for the density of the asthenosphere, in order to test the influence of
350 the buoyancy of the lithosphere on the rifting and the formation of rifted structures (Fig.
351 5). Thus, we compare three series of experiments with different lithosphere buoyancy
352 (see paragraph 3.2 for definition). The three values of buoyancy tested here are -30, 0
353 and +30 kg m⁻³. The model with a positive buoyancy (30 kg m⁻³) is the same as the
354 Mohr-Coulomb configuration described in paragraph 4.1.

355 Our first observation is that the variation of the buoyancy of the lithosphere does not
356 affect the timing of the break-up of the continental crust. Indeed, this break-up occurs
357 7 Ma after the beginning of the extension for all three models.

358 The strain rate patterns 0.5 Ma before the break-up of continental crust show an asym-
359 metry beneath the center of the rift zone for the two models with non-zero buoyancy
360 (Fig. 5A). This is probably due to the fact that the zero lithosphere buoyancy reduces
361 the mechanical contrast between the mantle lithosphere and the asthenosphere, avoiding
362 asymmetric processes to occur at this stage.

363 The geometry of the models at the moment of the continental crust break-up shows
364 a shallower boundary between mantle lithosphere and asthenosphere, as asthenosphere
365 density is lower than for the other tested models (Fig. 5A). This is simply due to the
366 fact that the lighter the material is, the more rapidly it uplifts. We observe that a zone
367 of possible partial melting occurs at the center of the rift for the model with a negative
368 buoyancy (-30 kg m^{-3}). Indeed, in this model the 1300°C isotherm (approximately the
369 base of the lithosphere) is shallow enough at the time of break-up of the continental
370 crust to allow for partial melting. This implies that oceanic crust can be produced at
371 this time, while magmatism may occur earlier, producing underplated and/or intruded
372 magma, as the continental crust is not yet broken apart. This process is characteristic of
373 the formation of volcanic passive margins.

374 Model geometries 18 Ma after the break-up of the continental crust show asymmetric
375 margins in all cases. We observe that the lateral position of the oceanic ridge is more
376 centered when buoyancy is negative (Fig. 5A-B, see also topographic profiles). Indeed,
377 predicted evolution of the topography shows that the oceanic ridge relocates after 10-

378 12 Ma for the model with positive buoyancy and after 6-7 Ma for the model with zero
379 buoyancy. The model with negative buoyancy shows an early relocation at the beginning
380 of the formation of the oceanic basin (Fig. 5C). We also observe that the depth of the
381 oceanic basin increases when asthenosphere is denser, which is consistent with the isostasy
382 effect, and that the model with a negative lithosphere buoyancy provides a better fit to
383 the present depth of the Gulf of Aden oceanic basin.

384 Thus, the buoyancy of the lithosphere controls (1) the depth of the oceanic basin, (2)
385 the position and the relocation of the oceanic ridge in the basin, and (3) the volcanic or
386 magma-poor nature of the rifted margins. A negative buoyancy of the lithosphere allows
387 for a depth of the oceanic basin comparable with observations in the eastern Gulf of Aden.

5. Discussion

5.1. Comparison to the eastern Gulf of Aden

388 The choice of parameters for this model is governed by the results of the parametric
389 study (failure criterion in the mantle lithosphere and buoyancy of the lithosphere) and the
390 geodynamic context (kinematics). Thus, we use a perfectly plastic mantle and a negative
391 lithosphere buoyancy of -20 kg m^{-3} , which is petrologically more realistic than the value
392 of -30 kg m^{-3} used in the parametric study. Then, we modify the boundary conditions
393 to better fit the actual kinematics (see Section 2): a velocity of 0.5 cm yr^{-1} is applied on
394 the left side (South), while a velocity of 1.5 cm yr^{-1} is applied on the right side (North),
395 to keep a total opening velocity of 2 cm yr^{-1} . The small initial thermal anomaly used
396 to localize the rift is set closer to the left side of the box, to ensure that the rift is at
397 the center of the box at the final stage (18 Ma after crustal break-up), comparable to the
398 present-day Gulf of Aden.

399 We compare the model at 18 Ma after the break-up of the continental crust to the data
400 available at the same scale in the eastern Gulf of Aden (Fig. 6). First, heat-flow at the
401 surface of the model is similar to heat-flow measurements for large wave-lengths on the
402 northern margin [Fig. 6A, *Lucazeau et al.*, 2008]. Next, geometry of the crustal thinning
403 is comparable with refraction and wide-angle reflection seismic velocity model along the
404 same line [Fig. 6B, *Leroy et al.*, 2010a]. However, the crude resolution of the model does
405 not allow for a more detailed match with the observed structures in the sediments and
406 crust. Finally, the topography of the model shows the same amplitude as profiles across
407 the eastern Gulf of Aden, even though the morphology of the rift shoulders is steeper than
408 the observation (Fig. 6C). The oceanic basin is also slightly deeper in the model than in
409 the data. In the eastern Gulf of Aden, higher than expected mantle heat-flow and lower
410 than expected seismic velocity and density values, inferred from wide-angle seismic and
411 gravity modeling, might be explained by a persistent post-rift thermal anomaly [*Lucazeau*
412 *et al.*, 2008; *Watremez et al.*, 2011a]. This topographic discrepancy might be explained by
413 the high thermal regime affecting the entire Gulf [e.g. *Lucazeau et al.*, 2008, 2009, 2010;
414 *d'Acremont et al.*, 2010; *Leroy et al.*, 2010b].

415 We also observe that pressure and temperature conditions in the asthenosphere at the
416 center of the rift allow for partial melting at the exact moment of the break-up of the
417 continental crust (Fig. 6B). The melt produced can infiltrate toward the surface and
418 either (1) become trapped beneath the margin (underplating, magmatism) to form a
419 volcanic margin and/or (2) generate oceanic crust, leaving very little time to serpentinize
420 or exhume continental mantle, forming a magma-poor margin. This is consistent with
421 the north-eastern Gulf of Aden margin that exhibits a very narrow OCT and even some

422 magmatism [*Autin et al.*, 2010; *Leroy et al.*, 2010a; *Watremez et al.*, 2011a; *Leroy et al.*,
423 2012], which may have triggered the continental break-up, as shown by *Bronner et al.*
424 [2011] for the Iberia margin.

5.2. Perfectly plastic failure criterion

425 The parametric study shows that a perfectly plastic mantle lithosphere allows for
426 stronger ridge relocation than a Mohr-Coulomb lithosphere, resulting in a ridge topogra-
427 phy more comparable to the present Gulf of Aden morphology.

428 The choice of the failure criterion in the mantle governs the deformation in the mantle
429 lithosphere and then the deformation in the continental crust. The perfectly plastic
430 criterion makes deformation more diffuse in the lithosphere, while deformation is more
431 localized with the Mohr-Coulomb mantle (narrower shear zones), using the same extension
432 velocity (or strain rate). This explains why the break-up of the continental crust occurs
433 earlier in the case of the Mohr-Coulomb mantle model.

434 These results are compatible with recent rheological and modeling studies [e.g.
435 *Kameyama et al.*, 1999; *Watts and Burov*, 2003; *Popov and Sobolev*, 2008], which propose
436 that a Mohr-Coulomb rheology (in the form of Byerlee's frictional plastic law) is less suit-
437 able for localized deformation of rocks in a high stress regime, especially in extension, than
438 Peierls or GBS rheologies. An alternative model advances the potential role of diking that
439 is supposed to weaken the lithosphere prior to rifting [e.g. *Buck*, 2004]. However, pre-rift
440 diking would lead to extensive pre-rift magmatism and formation of volcanic margins,
441 excluding the possibility to form a magma-poor rifted margin such as the eastern Gulf of
442 Aden.

5.3. Negative buoyancy of the continental lithosphere

443 The parametric study shows that the buoyancy of the mantle lithosphere has a strong
444 influence on the volcanic or magma-poor nature of the modeled rifted margin. Indeed, a
445 highly negatively buoyant mantle lithosphere (-30 kg m^{-3}) leads to the formation of melt
446 in the asthenosphere prior to crustal breakup, as observed along volcanic margins. On
447 the contrary, a greater buoyancy leads to the formation of typical magma-poor margins,
448 with a zone of exhumed continental mantle.

449 The comparison between observed and modeled Gulf of Aden topography suggests that
450 the mantle lithosphere of the Arabian shield has a negative buoyancy of approximately
451 -20 kg m^{-3} . Such values have also been proposed for the Baikal rift [*Gao et al.*, 1994;
452 *Petit and Déverchère*, 2006]. Moreover, thermodynamical modeling of the density for a
453 large mantle rock database has shown that mantle lithosphere of tectons can have slightly
454 negative buoyancy for conductive geotherms [*Griffin et al.*, 2009].

455 The assumption of a subcontinental lithosphere composition close to lherzolitic leads to
456 a positive buoyancy in the case of the Arabian shield (Fig. 3B), which is not in agreement
457 with the result of the models (Section 4.2). However, the heterogeneity and the complex
458 history of the mantle lithosphere are attested by many studies [*Kuo and Essene*, 1986;
459 *McGuire*, 1988; *Stein et al.*, 1993; *Nasir and Safarjalani*, 2000; *Kaliwoda et al.*, 2007;
460 *Shaw et al.*, 2007].

461 One can doubt the long-term stability of a continental lithosphere with negative buoy-
462 ancy with respect to the asthenosphere. In this case, we expect Rayleigh-Taylor instabili-
463 ties after 300-400 Ma, which lead to the collapse of the continental lithosphere [e.g. *Burov*
464 *and Watts*, 2006]. However, *Lenardic and Moresi* [1999] show that a positive buoyancy

465 of the lithosphere is not sufficient to create conditions for its long term stability. This
466 stability also depends on the strength of the lithosphere, an effective coupling between
467 the very buoyant crust and the mantle, as well as the occurrence of compressive stresses
468 [*François et al.*, in press]. The Arabian plate actually experienced such significant com-
469 pressive stresses due to successive subductions [*Al Hussein*, 2000], potentially explaining
470 why it did not collapse.

471 Similarly to our work, former observations and numerical models show that a negative
472 lithosphere buoyancy should lead to the development of Rayleigh-Taylor instabilities at
473 the mantle-asthenosphere boundary during the rifting, resulting in removal of an essential
474 amount of lithosphere mantle [e.g. *Burov*, 2007; *Van Wijk et al.*, 2008]. This has a strong
475 influence on the rifted structures.

6. Conclusions

476 The results of our modeling study show that the structure of the rifted continental
477 margins is highly sensitive to the failure criterion of the mantle lithosphere while the
478 buoyancy of the mantle lithosphere controls the depth of the oceanic basin and the relative
479 timing of the partial melting. The model using a perfectly plastic rheology and negatively
480 buoyant mantle lithosphere (-20 kg m^{-3}) shows similar features as the eastern Gulf of
481 Aden (heat-flow, topography, thinning of the continental crust, narrow OCT and position
482 of the ridge).

483 The perfectly plastic behavior represents a proxy for low temperature plasticity [e.g.
484 *Kameyama et al.*, 1999] whereas Mohr-Coulomb rheology produces higher stress and stress
485 drop, which best represents brittle behaviour at geodynamic time-scale. In the case of the
486 Gulf of Aden, structures are best fitted with a maximum yield strength of 450 MPa, which

487 is consistent with laboratory derived low temperature plasticity mechanism such as GBS
488 and Peierls creep [*Kameyama et al.*, 1999; *Précigout et al.*, 2007]. *Popov and Sobolev* [2008]
489 study, based on 3D model of continental rifting, argued that Mohr-Coulomb required
490 unrealistic stress build-up during continental rifting. Here, we reach similar conclusions
491 comparing our continental break-up model to the structures of the Gulf of Aden. Not
492 only, stress build-up is too strong, causing the formation of far too high rift shoulders
493 during continental rifting, but Mohr-Coulomb rheology also induced non realistic post-
494 rift topography and extremely long lasting initial phase of asymmetric spreading (10-12
495 Myr), which is neither observed in Aden nor anywhere else in world.

496 The Gulf of Aden represents the tipping point between the formation of (1) volcanic
497 rifted margins, where partial melting possibility occurs before the crustal break-up and
498 oceanic crust is created as soon as the continental crust is broken apart by dikes, and
499 (2) magma-poor rifted margins, where partial melting occurs after crustal break-up and a
500 zone of exhumed continental mantle forms between the last continental crust and the first
501 oceanic crust [e.g. *White and McKenzie*, 1989; *Whitmarsh et al.*, 1991; *Bauer et al.*, 2000].
502 Our parametric study shows that negatively buoyant lithosphere favors early occurrence
503 of melting, whereas neutrally to positively buoyant mantle lithosphere causes the melting
504 to be delayed by up to 1.5 Myr [*Watremez et al.*, 2011b]. Therefore, we posit that mantle
505 buoyancy variation could control the timing of melting and oceanization observed over a
506 wide range of passive margins. In the case of the Gulf of Aden, the first appearance of
507 partial melting in the rift is synchronous with the crustal break-up, which is shown to
508 correspond to a lithosphere that is negatively buoyant by a contrast of -20 kg m^{-3} . This
509 density contrast is confirmed by the petrological study of xenolith of the Arabian mantle

510 lithosphere and has also been shown to be a decisive factor for the occurrence of oceanic
511 obduction in North Oman using different boundary condition and numerical approach
512 [*Duretz et al.*, 2013].

513 This panel of evidences implies that the negatively buoyant mantle lithosphere of the
514 Arabian plate has been stable for several hundreds of million years. It rises the question
515 of the dynamic forces, which could be responsible for the long lasting stability and rapid
516 destabilization of old continental lithosphere at the onset of rifting. Further thermome-
517 chanical modeling of rifting, including petrological data to estimate the buoyancy of the
518 lithosphere and comparison to other geological region such as the Rio Grande Rift [*Song*
519 *and Helmberger*, 2007; *Van Wijk et al.*, 2008], are needed to better constrain the links
520 between partial melting and the rheology and buoyancy of continental mantle lithosphere
521 highlighted by our study.

522 **Acknowledgments.** The authors thank A. Popov, an anonymous reviewer and the
523 editor, T. Becker, for highly constructive comments. We also want to thank M. Cannat
524 and R. Huisman for helpful discussions. L.W. is grateful to her supervisors, K. Louden
525 and M. Nedimović, for their support during the preparation of this manuscript. L.W.
526 thanks K. Louden for help with proofreading. B.H. would like to thank T. Ntaflou for
527 the discussion on clinopyroxenites and J. Connolly for his answers concerning PERPLEX.
528 Figure 1 has been produced using the GMT package [*Wessel and Smith*, 1995]. The ANR
529 Rift2Ridge, YOCMAL, CNRS-INSU and Action Marges provided the financial support
530 for this study.

References

- 531 Agard, P., M. P. Searle, G. I. Alsop, and B. Dubacq (2010), Crustal stacking and expul-
532 sion tectonics during continental subduction: P-T deformation constraints from Oman,
533 *Tectonics*, *29*(5), 19 p.
- 534 Ahmed, A., C. Tiberi, S. Leroy, G. Stuart, D. Keir, J. Sholan, K. Khanbari, I. Al-
535 Ganad, and C. Basuyau (2013), Crustal structure of the rifted volcanic margins and
536 uplifted plateau of Western Yemen from receiver function analysis, *Geophys. J. Int.*,
537 doi:10.1093/gji/ggt072.
- 538 Al Amri, A. M. S. (1999), The crustal and upper-mantle structure of the interior Arabian
539 Platform, *Geophys. J. Int.*, *136*, 421–430.
- 540 Al-Damegh, K., E. Sandvol, and M. Barazangi (2005), Crustal structure of the Arabian
541 plate: new constraints from the analysis of teleseismic receiver functions, *Earth Planet.*
542 *Sci. Lett.*, *231*(3-4), 177–196.
- 543 Al-Hashmi, S., R. Gök, K. Al-Toubi, Y. Al-Shijbi, I. El-Hussain, and A. J. Rodgers (2011),
544 Seismic velocity structure at the southern margin of the Arabian Peninsula, *Geophys.*
545 *J. Int.*, *186*(2), 782–792.
- 546 Al Hussein, M. I. (2000), Origin of the Arabian Plate structures; Amar collision and Najd
547 Rift, *GeoArabia*, *5*(4), 527–542.
- 548 Al-Lazki, A., C. Ebinger, M. Kendall, G. Hellfrich, S. Leroy, C. Tiberi, G. Stuart, and
549 K. Al-Toubi (2012), Upper mantle anisotropy of southeast Arabia passive margin (Gulf
550 of Aden northern conjugate margin), Oman., *Arab. J. Geosci.*, *5*(5), 925–934, doi:
551 10.1007/s12517-011-0477-2.

- 552 Autin, J., S. Leroy, E. d'Acremont, M.-O. Beslier, A. Ribodetti, N. Bellahsen, P. Razin,
553 and C. Robin (2010), Continental break-up history of a deep magma-poor margin from
554 seismic reflection data (northeastern Gulf of Aden margin, offshore Oman), *Geophys.*
555 *J. Int.*, *180*, 501–519.
- 556 Bassi, G. (1995), Relative importance of strain rate and rheology for the mode of conti-
557 nental extension, *Geophys. J. Int.*, *122*(1), 195–210.
- 558 Basuyau, C., C. Tiberi, S. Leroy, G. Stuart, A. I. Al-Lazki, K. Al-Toubi, and C. Ebinger
559 (2010), Evidence of partial melting beneath a continental margin: case of Dhofar, in
560 the Northern Gulf of Aden (Sultanate of Oman), *Geophys. J. Int.*, *180*, 520–534.
- 561 Bauer, K., S. Neben, B. Schreckenberger, R. Emmermann, K. Hinz, N. Fechner, K. Gohl,
562 A. Schulze, R. Trumbull, and K. Weber (2000), Deep structure of the Namibia continen-
563 tal margin as derived from integrated geophysical studies, *J. Geophys. Res.*, *105*(B11),
564 25,829–25,853.
- 565 Boillot, G., M. Recq, E. Winterer, A. Meyer, J. Applegate, M. Baltuck, J. Bergen, M. Co-
566 mas, T. Davies, K. Dunham, et al. (1987), Tectonic denudation of the upper mantle
567 along passive margins: a model based on drilling results (ODP Leg 103, western Galicia
568 margin, Spain), *Tectonophysics*, *132*(4), 335–342.
- 569 Bosence, D. (1997), Mesozoic rift basins of Yemen, *Mar. Pet. Geol.*, *14*(6), 611.
- 570 Bronner, A., D. Sauter, G. Manatschal, G. Péron-Pinvidic, and M. Munsch (2011),
571 Magmatic breakup as an explanation for magnetic anomalies at magma-poor rifted
572 margins, *Nat. Geosci.*, *4*(8), 549–553.
- 573 Brun, J.-P., and M.-O. Beslier (1996), Mantle exhumation at passive margins, *Earth*
574 *Planet. Sci. Lett.*, *142*(1-2), 161–173.

- 575 Buck, W. (2004), Consequences of athenospheric variability on continental rifting, in
576 *Rheology and Deformation of the Lithosphere at continental margins*, vol. 62, edited
577 by G. D. Karner, B. Taylor, N. W. Driscoll, and D. L. Kohlstedt, pp. 1–30, Columbia
578 University Press.
- 579 Bürgmann, R., and G. Dresen (2008), Rheology of the lower crust and upper mantle: Ev-
580 idence from rock mechanics, geodesy, and field observations, *Annu. Rev. Earth Planet.*
581 *Sci.*, *36*, 531–567.
- 582 Burov, E. (2011), Rheology and strength of the lithosphere, *Mar. Pet. Geol.*, *28*(8), 1402–
583 1443.
- 584 Burov, E., and M. Diament (1995), The effective elastic thickness (T_e) of continental
585 lithosphere: What does it really mean?, *J. Geophys. Res.*, *100*(B3), 3905–3927.
- 586 Burov, E., and P. Yamato (2008), Continental plate collision, PTtz conditions and un-
587 stable vs. stable plate dynamics: insights from thermo-mechanical modelling, *Lithos*,
588 *103*(1-2), 178–204.
- 589 Burov, E. B. (2007), The role of gravitational instabilities, density structure and extension
590 rate in the evolution of continental margins, *Geol. Soc. Spec. Publ.: Imaging, Mapping*
591 *and Modelling Continental Lithosphere Extension and Breakup*, *282*, 139–156.
- 592 Burov, E. B., and S. A. P. L. Cloetingh (2009), Controls of mantle plumes and lithospheric
593 folding on modes of intra-plate continental tectonics: differences and similarities, *Geo-*
594 *phys. J. Int.*, *178*, 1691–1722.
- 595 Burov, E. B., and A. Poliakov (2001), Erosion and rheology controls on syn and post-
596 rift evolution: verifying old and new ideas using a fully coupled numerical model., *J.*
597 *Geophys. Res.*, *106*(B8), 16,461–16,481.

- 598 Burov, E. B., and A. B. Watts (2006), The long-term strength of continental lithosphere:
599 "jelly-sandwich" or "crème-brûlée"?, *GSA Today*, *16*, 4–10.
- 600 Byerlee, J. (1978), Friction of rocks, *Pure Appl. Geophys.*, *116*(4), 615–626.
- 601 Chang, S., and S. Van der Lee (2011), Mantle plumes and associated flow beneath Arabia
602 and East Africa, *Earth Planet. Sci. Lett.*, *302*(3-4), 448–454.
- 603 Chéry, J., M. Daignières, F. Lucazeau, and J. Vilotte (1989), Strain localization in rift
604 zones (case of a thermally softened lithosphere): a finite element approach, *Bull. Soc.*
605 *Geol. Fr.*, *8*, 437–443.
- 606 Connolly, J. (2009), The geodynamic equation of state: what and how, *Geochem. Geophys.*
607 *Geosyst.*, *10*, Q10,014.
- 608 Contrucci, I., L. Matias, M. Moulin, L. Géli, F. Klingelhofer, H. Nouzé, D. Aslanian, J. L.
609 Olivet, J. P. Réhault, and J. C. Sibuet (2004), Deep structure of the West African con-
610 tinental margin (Congo, Zaire, Angola), between 5 S and 8 S, from reflection/refraction
611 seismics and gravity data, *Geophys. J. Int.*, *158*(2), 529–553.
- 612 Courtillot, V., C. Jaupart, I. Manighetti, P. Tapponnier, and J. Besse (1999), On causal
613 links between flood basalts and continental breakup, *Earth Planet. Sci. Lett.*, *166*(3-4),
614 177–195.
- 615 Culling, W. (1960), Analytical theory of erosion, *J. Geol.*, *68*, 336–344.
- 616 Cundall, P. (1989), Numerical experiments on localization in frictional materials, *Arch.*
617 *Appl. Mech.*, *59*(2), 148–159.
- 618 Debayle, E., J. L eveque, and M. Cara (2001), Seismic evidence for a deeply rooted low-
619 velocity anomaly in the upper mantle beneath the northeastern Afro/Arabian continent,
620 *Earth Planet. Sci. Lett.*, *193*(3-4), 423–436.

- 621 Denele, Y., S. Leroy, E. Pelleter, R. Pik, J.-Y. Talbot, and K. Khanbari (2012), The
622 Cryogenian juvenile arc formation and successive high-K calc-alkaline plutons intrusion
623 of Socotra island (Yemen), *Arab. J. Geosci.*, *5*(5), 903–924, doi:10.1007/s12517-011-
624 0476-3.
- 625 d’Acremont, E., S. Leroy, M. Maia, P. Patriat, O. Beslier Marie, N. Bellahsen, M. Fournier,
626 and P. Gente (2006), Structure and evolution of the eastern Gulf of Aden; insights from
627 magnetic and gravity data (Encens-Sheba MD117 cruise), *Geophys. J. Int.*, *165*(3),
628 786–803.
- 629 d’Acremont, E., S. Leroy, M. Maia, P. Gente, and J. Autin (2010), Volcanism, jump and
630 propagation on the Sheba Ridge, eastern Gulf of Aden: Segmentation evolution and
631 implications for accretion processes, *Geophys. J. Int.*, *180*, 535–551.
- 632 Duretz, T., P. Agard, P. Yamato, T. Gerya, and E. Burov (2013), Obduction at plate
633 boundaries : thermo-mechanical modelling, *Geophys. Res. Abstracts*, *Vol. 15*(33),
634 EGU2013–9724.
- 635 Eldholm, O., and K. Grue (1994), North Atlantic volcanic margins: dimensions and
636 production rates, *J. Geophys. Res.*, *99*(B2), 2955–2968.
- 637 Farr, T., P. Rosen, E. Caro, R. Crippen, R. Duren, S. Hensley, M. Kobrick, M. Paller,
638 E. Rodriguez, L. Roth, et al. (2007), The shuttle radar topography mission, *Rev. Geo-*
639 *phys.*, *45*(2), 33.
- 640 Fournier, M., P. Patriat, and S. Leroy (2001), Reappraisal of the Arabia–India–Somalia
641 triple junction kinematics, *Earth Planet. Sci. Lett.*, *189*(3-4), 103–114.
- 642 François, T., E. B. Burov, B. Meyer, and P. Agard (in press), Surface topogra-
643 phy as key constraint on thermo-reological structure of cratons, *Tectonophysics*, doi:

- 644 10.1016/j.tecto.2012.10.009.
- 645 Frisch, W., and A. Al-Shanti (1977), Ophiolite belts and the collision of island arcs in the
646 Arabian Shield, *Tectonophysics*, *43*(3-4), 293–306.
- 647 Gao, S., P. Davis, H. Liu, P. Slack, Y. Zorin, N. Logatchev, M. Kogan, P. Burkholder,
648 and R. Meyer (1994), Asymmetric upwarp of the asthenosphere beneath the Baikal rift
649 zone, Siberia, *J. Geophys. Res.*, *99*, 15–319.
- 650 Geoffroy, L. (2005), Volcanic passive margins, *C. R. Géoscience*, *337*(16), 1395–1408.
- 651 Gerlings, J., K. Louden, and H. Jackson (2011), Crustal structure of the Flemish Cap Con-
652 tinental Margin (eastern Canada): an analysis of a seismic refraction profile, *Geophys.*
653 *J. Int.*, *185*(1), 30–48.
- 654 Gerya, T., L. Perchuk, and J. Burg (2008), Transient hot channels: perpetrating and
655 regurgitating ultrahigh-pressure, high-temperature crust-mantle associations in collision
656 belts, *Lithos*, *103*(1-2), 236–256.
- 657 Griffin, W., S. O'Reilly, J. Afonso, and G. Begg (2009), The composition and evolution
658 of lithospheric mantle: a re-evaluation and its tectonic implications, *J. Petrol.*, *50*(7),
659 1185.
- 660 Griffin, W. L., S. Y. O'Reilly, N. Abe, S. Aulbach, R. M. Davies, N. J. Pearson, B. J.
661 Doyle, and K. Kivi (2003), The origin and evolution of Archean lithospheric mantle,
662 *Precambrian Res.*, *127*, 19–41.
- 663 Hager, B., and M. Richards (1989), Long-wavelength variations in Earth's geoid: physical
664 models and dynamical implications, *Philos. T. Roy. Soc. A*, *328*, 309–327.
- 665 Hargrove, U., R. Stern, J. Kimura, W. Manton, and P. Johnson (2006), How juvenile is the
666 Arabian-Nubian Shield? Evidence from Nd isotopes and pre-Neoproterozoic inherited

667 zircon in the Bi'r Umq suture zone, Saudi Arabia, *Earth Planet. Sci. Lett.*, 252(3-4),
668 308–326.

669 Henjes-Kunst, F., R. Altherr, and A. Baumann (1990), Evolution and composition of the
670 lithospheric mantle underneath the western Arabian peninsula: constraints from Sr- Nd
671 isotope systematics of mantle xenoliths, *Contrib. Mineral. Petrol.*, 105(4), 460–472.

672 Hirth, G., and D. Kohlstedt (2003), Rheology of the upper mantle and the mantle wedge:
673 A view from the experimentalists, *Geophys. Monogr.*, 138, 83–105.

674 Hofmann, A., and W. White (1982), Mantle plumes from ancient oceanic crust, *Earth*
675 *Planet. Sci. Lett.*, 57(2), 421–436.

676 Huismans, R., and C. Beaumont (2011), Depth-dependent extension, two-stage breakup
677 and cratonic underplating at rifted margins, *Nature*, 473(7345), 74–78.

678 Huismans, R. S., and C. Beaumont (2003), Symmetric and asymmetric lithospheric exten-
679 sion; relative effects of frictional-plastic and viscous strain softening, *J. Geophys. Res.*,
680 108(B10), 2496–2508.

681 Kaliwoda, M., R. Altherr, and H. Meyer (2007), Composition and thermal evolution of
682 the lithospheric mantle beneath the Harrat Uwayrid, eastern flank of the Red Sea rift
683 (Saudi Arabia), *Lithos*, 99(1-2), 105–120.

684 Kameyama, M., D. Yuen, and S. Karato (1999), Thermal-mechanical effects of low-
685 temperature plasticity (the Peierls mechanism) on the deformation of a viscoelastic
686 shear zone, *Earth Planet. Sci. Lett.*, 168(1-2), 159–172.

687 Kaus, B., J. Connolly, Y. Podladchikov, and S. Schmalholz (2005), Effect of mineral phase
688 transitions on sedimentary basin subsidence and uplift, *Earth Planet. Sci. Lett.*, 233(1),
689 213–228.

- 690 Kuo, L., and E. Essene (1986), Petrology of spinel harzburgite xenoliths from the Kishb
691 Plateau, Saudi Arabia, *Contrib. Mineral. Petrol.*, *93*(3), 335–346.
- 692 Lavier, L., and G. Manatschal (2006), A mechanism to thin the continental lithosphere
693 at magma-poor margins, *Nature*, *440*(7082), 324–8.
- 694 Le Pourhiet, L. (2013), Strain Localization Due to Structural Softening During Pressure
695 Sensitive Rate Independent Yielding, *Bull. Soc. Geol. Fr.*, *184*(3).
- 696 Lenardic, A., and L. Moresi (1999), Some thoughts on the stability of cratonic lithosphere-
697 Effects of buoyancy and viscosity, *J. Geophys. Res.*, *104*(B6), 12,747–12,759.
- 698 Leroy, S., P. Gente, M. Fournier, E. d’Acremont, P. Patriat, M.-O. Beslier, N. Bellahsen,
699 M. Maia, A. Blais, J. Perrot, A. Al Kathiri, S. Merkouriev, J.-M. Fleury, P.-Y. Ruellan,
700 C. Lepvrier, and P. Huchon (2004), From rifting to spreading in the eastern Gulf of
701 Aden; a geophysical survey of a young oceanic basin from margin to margin, *Terra
702 Nova*, *16*(4), 185–192.
- 703 Leroy, S., F. Lucazeau, E. d’Acremont, L. Watremez, J. Autin, S. Rouzo, N. Bellahsen,
704 C. Tiberi, C. Ebinger, M.-O. Beslier, J. Perrot, P. Razin, F. Rolandone, H. Sloan,
705 G. Stuart, A. Al Lazki, K. Al-Toubi, F. Bache, A. Bonneville, B. Goutorbe, P. Huchon,
706 P. Unternehr, and K. Khanbari (2010a), Contrasted styles of rifting in the eastern Gulf
707 of Aden: A combined wide-angle, multichannel seismic, and heat flow survey, *Geochem.
708 Geophys. Geosyst.*, *11*, Q07,004.
- 709 Leroy, S., E. d’Acremont, C. Tiberi, C. Basuyau, J. Autin, F. Lucazeau, and H. Sloan
710 (2010b), Recent off-axis volcanism in the eastern Gulf of Aden: implications for plume-
711 ridge interaction, *Earth Planet. Sci. Lett.*, *293*, 140–153.

- 712 Leroy, S., P. Razin, J. Autin, F. c. Bache, E. d'Acremont, L. Watremez, J. Robinet,
713 C. Baurion, Y. Denèle, N. Bellahsen, F. Lucazeau, F. Rolandone, S. Rouzo, J. Serra Kiel,
714 C. Robin, F. c. Guillocheau, C. Tiberi, C. Basuyau, M.-O. Beslier, C. Ebinger, G. Stuart,
715 A. Ahmed, K. Khanbari, I. Al-Ganad, P. de Clarens, P. Unternehr, K. Al-Toubi, and
716 A. Al-Lazki (2012), From rifting to oceanic spreading in the Gulf of Aden: a synthesis,
717 *Arab. J. Geosci.*, 5(5), 859–901, doi:10.1007/s12517-011-0475-4.
- 718 Lithgow-Bertelloni, C., and P. G. Silver (1998), Dynamic topography, plate driving forces
719 and the African superswell, *Nature*, 395(6699), 269–272.
- 720 Little, T., M. Savage, and B. Tikoff (2002), Relationship between crustal finite strain and
721 seismic anisotropy in the mantle, Pacific–Australia plate boundary zone, South Island,
722 New Zealand, *Geophys. J. Int.*, 151(1), 106–116.
- 723 Louden, K., J. Sibuet, and F. Harmegnies (1997), Variations in heat flow across the
724 ocean-continent transition in the Iberia abyssal plain, *Earth Planet. Sci. Lett.*, 151(3-
725 4), 233–254.
- 726 Lucazeau, F., S. Leroy, A. Bonneville, B. Goutorbe, F. Rolandone, E. d'Acremont, L. Wa-
727 tremez, D. Düsünur, P. Tuchais, P. Huchon, N. Bellahsen, and K. Al-Toubi (2008), Per-
728 sistent thermal activity at the Eastern Gulf of Aden after continental break-up, *Nat.*
729 *Geosci.*, 1, 854–858.
- 730 Lucazeau, F., S. Leroy, J. Autin, A. Bonneville, B. Goutorbe, L. Watremez,
731 E. d'Acremont, D. Düsünur, F. Rolandone, and P. Huchon (2009), Post-rift volcan-
732 ism and high heat-flow at the Ocean-Continent Transition of the Gulf of Aden, *Terra*
733 *Nova*, 21, 285–292.

- 734 Lucazeau, F., S. Leroy, F. Rolandone, E. d'Acremont, L. Watremez, A. Bonneville,
735 B. Goutorbe, and D. Düsünur (2010), Heat-flow and hydrothermal circulations at the
736 Ocean-Continent Transition of the Eastern Gulf of Aden., *Earth Planet. Sci. Lett.*, *295*,
737 554–570.
- 738 Manatschal, G. (2004), New models for evolution of magma-poor rifted margins based on
739 a review of data and concepts from West Iberia and the Alps, *Int. J. Earth Sci.*, *93*(3),
740 432–466.
- 741 McGuire, A. (1988), Petrology of mantle xenoliths from Harrat al Kishb: the mantle
742 beneath western Saudi Arabia, *J. Petrol.*, *29*(1), 73.
- 743 McKenzie, D., and M. Bickle (1988), The volume and composition of melt generated by
744 extension of the lithosphere, *J. Petrol.*, *29*(3), 625.
- 745 Minshull, T. (2002), Seismic Structure of the Oceanic Crust and Passive Continental
746 Margins, *International Handbook of Earthquake and Engineering Seismology*, *81A*, 911–
747 924.
- 748 Mjelde, R., T. Raum, Y. Murai, and T. Takanami (2007), Continent-ocean-transitions:
749 Review, and a new tectono-magmatic model of the Vøring Plateau, NE Atlantic, *J.*
750 *Geodyn.*, *43*(3), 374–392.
- 751 Molnar, P., H. Anderson, E. Audoine, D. Eberhart-Phillips, K. Gledhill, E. Klosko,
752 T. McEvilly, D. Okaya, M. Savage, T. Stern, et al. (1999), Continuous deformation
753 versus faulting through the continental lithosphere of New Zealand, *Science*, *286*(5439),
754 516–519.
- 755 Mooney, W., M. Gettings, H. Blank, and J. Healy (1985), Saudi Arabian seismic-refraction
756 profile: A travelttime interpretation of crustal and upper mantle structure, *Tectono-*

- 757 *physics*, 111(3-4), 173–197.
- 758 Moulin, M., D. Aslanian, J. Olivet, I. Contrucci, L. Matias, L. Geli, F. Klingelhoefer,
759 H. Nouze, J. Rehaul, and P. Unternehr (2005), Geological constraints on the evolution
760 of the Angolan margin based on reflection and refraction seismic data (ZaiAngo project),
761 *Geophys. J. Int.*, 162(3), 793–810.
- 762 Mutter, J., M. Talwani, and P. Stoffa (1982), Origin of seaward-dipping reflectors in
763 oceanic crust off the Norwegian margin by “subaerial sea-floor spreading”, *Geology*,
764 10(7), 353–357.
- 765 Nasir, S., and A. Safarjalani (2000), Lithospheric petrology beneath the northern part
766 of the Arabian Plate in Syria: evidence from xenoliths in alkali basalts, *J. Afr. Earth.*
767 *Sci.*, 30(1), 149–168.
- 768 O'Neill, C., L. Moresi, D. Müller, R. Albert, and F. Dufour (2006), Ellipsis 3D: A particle-
769 in-cell finite-element hybrid code for modelling mantle convection and lithospheric de-
770 formation, *Computers & geosciences*, 32(10), 1769–1779.
- 771 Pasyanos, M., and A. Nyblade (2007), A top to bottom lithospheric study of Africa and
772 Arabia, *Tectonophysics*, 444(1-4), 27–44.
- 773 Pasyanos, M. E., and W. R. Walter (2002), Crust and upper-mantle structure of North
774 Africa, Europe and the Middle East from inversion of surface waves, *Geophys. J. Int.*,
775 149, 463–481.
- 776 Pérez-Gussinyé, M., and T. Reston (2001), Rheological evolution during extension at
777 nonvolcanic rifted margins: Onset of serpentinization and development of detachments
778 leading to continental breakup, *J. Geophys. Res.*, 106(B3), 3961–3976.

- 779 Petit, C., and J. Déverchère (2006), Structure and evolution of the Baikal rift: a synthesis,
780 *Geochem. Geophys. Geosyst.*, 7(11), Q11,016.
- 781 Poliakov, A., P. Cundall, Y. Podladchikov, and V. Lyakhovsky (1993), *Flow and Creep in*
782 *the Solar System: observations, modeling and theory*, chap. An explicit inertial method
783 for the simulation of viscoelastic flow: an evaluation of elastic effects on diapiric flow in
784 two-and three-layers models, pp. 175–195, Kluwer Academic Publishers.
- 785 Popov, A., and S. Sobolev (2008), SLIM3D: A tool for three-dimensional thermomechanical
786 modeling of lithospheric deformation with elasto-visco-plastic rheology, *Phys. Earth*
787 *Planet. In.*, 171(1-4), 55–75.
- 788 Précigout, J., F. Gueydan, D. Gapais, C. Garrido, and A. Essaifi (2007), Strain localisation
789 in the subcontinental mantle – ductile alternative to the brittle mantle, *Tectonophysics*,
790 445(3-4), 318–336.
- 791 Ranalli, G. (1995), *Rheology of the Earth (2nd edit.)*, Chapman & Hall, London.
- 792 Ritsema, J., and H. van Heijst (2000), New seismic model of the upper mantle beneath
793 Africa, *Geology*, 28(1), 63–66.
- 794 Saleeby, J., M. Ducea, and D. Clemens-Knott (2003), Production and loss of high-density
795 batholithic root, southern Sierra Nevada, California., *Tectonics*, 22, 1064.
- 796 Sandvol, E., D. Seber, M. Barazangi, F. Vernon, J. Mellors Robert, and M. S. Al Amri Ab-
797 dullah (1998), Lithospheric seismic velocity discontinuities beneath the Arabian Shield,
798 *Geophys. Res. Lett.*, 25(15), 2873–2876.
- 799 Sandwell, D., and W. Smith (1997), Marine gravity anomaly from Geosat and ERS 1
800 satellite altimetry, *J. Geophys. Res.*, 102(10), 039–10.

- 801 Searle, M. (1983), Stratigraphy, structure and evolution of the Tibetan-Tethys zone in
802 Zaskar and the Indus suture zone in the Ladakh Himalaya, *Trans. R. Soc. Edinburgh*
803 *Earth Sci*, 73, 205–219.
- 804 Shaw, J., J. Baker, A. Kent, K. Ibrahim, and M. Menzies (2007), The Geochemistry of
805 the Arabian Lithospheric Mantle Source for Intraplate Volcanism?, *J. Petrol.*, 48(8),
806 1495.
- 807 Sibuet, J. C., S. Srivastava, and G. Manatschal (2007), Exhumed mantle-forming tran-
808 sitional crust in the Newfoundland-Iberia rift and associated magnetic anomalies, *J.*
809 *Geophys. Res.*, 112(B6), 06,105.
- 810 Sobolev, A., A. Hofmann, D. Kuzmin, G. Yaxley, N. Arndt, S. Chung, L. Danyushevsky,
811 T. Elliott, F. Frey, M. Garcia, et al. (2007), The amount of recycled crust in sources of
812 mantle-derived melts, *Science*, 316(5823), 412–417.
- 813 Sol, S., A. Meltzer, R. Bürgmann, R. Van der Hilst, R. King, Z. Chen, P. Koons, E. Lev,
814 Y. Liu, P. Zeitler, et al. (2007), Geodynamics of the southeastern Tibetan Plateau from
815 seismic anisotropy and geodesy, *Geology*, 35(6), 563–566.
- 816 Song, T.-R. A., and D. Helmberger (2007), A depleted, destabilized continental lithosphere
817 near the Rio Grande rift, *Earth and Planetary Science Letters*, 262(1), 175–184.
- 818 Srivastava, S., and W. Roest (1995), Nature of Thin Crust Across the Southwest Green-
819 land Margin and its Bearing on the Location of the Ocean-Continent Boundary, *Pro-*
820 *ceedings of the NATO-ARW Workshop on Rifted Ocean-Continent Boundaries, 11-14*
821 *May, 1994, Mallorca, Spain, Kluwer Academic, Dordrecht*, 1, 95–120.
- 822 Stein, M., Z. Garfunkel, and E. Jagoutz (1993), Chronothermometry of peridotitic and
823 pyroxenitic xenoliths: Implications for the thermal evolution of the Arabian lithosphere,

- 824 *Geochim. Cosmochim. Ac.*, 57(6), 1325–1337.
- 825 Tiberi, C., S. Leroy, E. d’Acremont, N. Bellahsen, C. Ebinger, A. Al Lazki, and A. Pointu
826 (2007), Crustal geometry of the northeastern Gulf of Aden passive margin; localization
827 of the deformation inferred from receiver function analysis, *Geophys. J. Int.*, 168(3),
828 1247–1260.
- 829 Turcotte, D., and G. Schubert (2002), *Geodynamics*, Cambridge University Press.
- 830 Unternehr, P., G. Pron-Pinvidic, G. Manatschal, and E. Sutra (2010), Hyper-extended
831 crust in the South Atlantic: in search of a model, *Pet. Geosci.*, 16, 207–215, doi:
832 10.1144/SP369.10.
- 833 van Hunen, J., A. Van Den Berg, and N. Vlaar (2002), On the role of subducting oceanic
834 plateaus in the development of shallow flat subduction, *Tectonophysics*, 352(3-4), 317–
835 333.
- 836 Van Wijk, J., and S. Cloetingh (2002), Basin migration caused by slow lithospheric ex-
837 tension, *Earth and Planetary Science Letters*, 198(3), 275–288.
- 838 Van Wijk, J., J. Van Hunen, and S. Goes (2008), Small-scale convection during continental
839 rifting: Evidence from the Rio Grande rift, *Geology*, 36(7), 575–578.
- 840 Vermeer, P. (1990), Orientation of shear bands in biaxial tests, *Geotechnique*, 40(2), 223–
841 236.
- 842 Vigny, C., P. Huchon, J. Ruegg, K. Khanbari, and L. Asfaw (2006), Confirmation of
843 Arabia slow plate motion by new GPS data in Yemen, *J. Geophys. Res.*, 111(B2),
844 B02,402.
- 845 Wallace, M., and D. Green (1991), The effect of bulk rock composition on the stabil-
846 ity of amphibole in the upper mantle: implications for solidus positions and mantle

- 847 metasomatism, *Miner. Petrol.*, *44*(1), 1–19.
- 848 Watremez, L., S. Leroy, S. Rouzo, E. d’Acremont, P. Unternehr, C. Ebinger, F. Lucazeau,
849 and A. Al Lazki (2011a), The crustal structure of the north eastern Gulf of Aden
850 continental margin: insights from wide angle seismic data, *Geophys. J. Int.*, *184*(2),
851 575–574.
- 852 Watremez, L., E. B. Burov, E. d’Acremont, S. Leroy, and B. Huet (2011b), Mantle densities
853 and rupture criterion: thermo-mechanical modelling applied to the Eastern Gulf of
854 Aden, *Geophys. Res. Abstracts*, *Vol. 13*(33), EGU2011–9235.
- 855 Watts, A., and E. Burov (2003), Lithospheric strength and its relationship to the elastic
856 and seismogenic layer thickness, *Earth Planet. Sci. Lett.*, *213*(1-2), 113–131.
- 857 Wessel, P., and W. Smith (1995), New version of the Generic Mapping Tools released,
858 *Eos Trans. AGU*, *76*(33), 329.
- 859 White, R., and D. McKenzie (1989), Magmatism at Rifts zones: the generation of volcanic
860 continental margin and flood basalts, *J. Geophys. Res.*, *94*(1), 7685–7730.
- 861 Whitmarsh, R., P. Miles, L. Pinheiro, G. Boillot, and M. Recq (1991), The ocean-continent
862 transition of western Iberia, *Geobyte*, *75*(8), 1425.
- 863 Xu, W., C. Lithgow-Bertelloni, L. Stixrude, and J. Ritsema (2008), The effect of bulk
864 composition and temperature on mantle seismic structure, *Earth Planet. Sci. Lett.*,
865 *275*(1-2), 70–79.
- 866 Yamato, P., P. Agard, E. Burov, L. Le Pourhiet, L. Jolivet, and C. Tiberi (2007), Burial
867 and exhumation in a subduction wedge: Mutual constraints from thermomechanical
868 modeling and natural PTt data (Schistes Lustres, western Alps), *J. geophys. Res.*, *112*,
869 B07,410.

Figure 1. Geodynamic settings of the Gulf of Aden.

Arrows show GPS vectors considering the Eurasian plate fixed [from *Vigny et al.*, 2006]; numbers are the velocities in mm/yr. Black dots are epicentres of earthquakes (USGS database from 1973/01 to 2011/04, $M_W \geq 3.5$ - <http://earthquake.usgs.gov/earthquakes/eqarchives/epic/>). Hatched areas correspond to the Arabo-Nubian shield. Abbreviations: AFTZ, Alula-Fartak Transform Zone; AR, Aden Ridge; CR, Carlsberg Ridge; EAR: East African Rift; OFZ, Owen Fracture Zone; SHTZ, Socotra-Hadbeen Transform Zone; SR, Sheba Ridge; SSFZ, Shukra-el-Sheik Fracture Zone. The direction of extension of the Gulf of Aden is highlighted by the orientation of the transform zones. Relief is compiled from SRTM topography data [*Farr et al.*, 2007] and gravity-predicted bathymetry [*Sandwell and Smith*, 1997].

Figure 2. Model setup.

An extension velocity of 1 cm/yr is applied on each side of the model. The springs represent the lithostatic pressure (Winkler basement) that is applied at the base of the model. The strength envelopes (blue and red curves) compare the different rheological behaviour in depth for the two different mantle failure criteria in the upper 150 km of the model. The black curve presents the evolution of the temperature with depth in the upper 150 km of the model. A 50°C thermal anomaly is applied at the base of the crust to localize the deformation at the center of the model.

Figure 3. The Arabian plate mantle lithosphere buoyancy.

A. Composition of xenoliths from the Arabian plate mantle lithosphere (see Supplementary material for the references), of subcontinental mantle lithosphere standards from four tectons [*Griffin et al.*, 2009] and of the fertile Hawaiian pyrolite standard [*Wallace and Green*, 1991] plotted in a Mg# vs. %Al₂O₃ diagram (Mg#=100 Mg/(Mg+Fe)). Also shown is the range of the tecton xenolith suites [*Griffin et al.*, 2009]. Two groups of xenoliths can be separated according to their chemistry. Lherzolites (lhz) and harzburgites (haz) have low Al₂O₃ content and high Mg#. In spite of the scattering, clinopyroxenites (cpx) and websterites (web) have high Al₂O₃ content and low Mg#.

B. Buoyancy calculated for the compositions of the xenoliths and the tecton standards along the initial thermal profile of the model (the buoyancy is calculated relative to the asthenosphere). The rapid buoyancy decrease between 50 km and 80 km shown by several curves of the cpx-web group corresponds to the plagioclase-spinel-garnet transitions.

C. Calculation of the Arabian plate mantle lithosphere buoyancy as a mixing of depleted and fertile rocks. The depleted fractions correspond to either the mean lhz-haz group (mean buoyancy $\sim 20 \text{ kg m}^{-3}$) or the mean of the tecton standards (mean buoyancy $\sim 5 \text{ kg m}^{-3}$). The fertile fraction corresponds to the cpx-web group (mean buoyancy $\sim 100 \text{ kg m}^{-3}$). The buoyancy decreases with increasing fraction of cpx-web. The density of the “best fit model” ($\sim 20 \text{ kg m}^{-3}$, see section 5.1) can be achieved for a mantle lithosphere containing approximately 30% clinopyroxenite and websterite.

Figure 4. Influence of the mantle lithosphere rheology.

The two columns correspond to the results of the two models comparing mantle lithosphere rheology.

A. The first line shows the strain rate in the models 0.5 Ma before the break-up of the continental crust, respecting the color scale shown below. The second and third lines show the geometry of the model at the time of the break-up of the continental crust and 18 Ma later, respectively. The color code for the materials is the same as in Figure 2. The black arrows show the position of the oceanic spreading ridge.

B. Topography of the models at the moment of crustal break-up and 18 Ma afterwards compared with the present-day topography of the Gulf of Aden.

C. Evolution of the model topography through time: at each time line correspond a 2D topographic line. Left panel: Mohr-Coulomb model. Right panel: Perfectly-plastic model (following the columns of panel A). The higher elevations (dark red) show the positions of the rift shoulders through time while the narrow green-to-blue zone shows the position of the oceanic ridge. The black circles highlight the places where and times when the oceanic ridge relocates (ridge jumps). The black horizontal lines correspond to the moment of crustal break-up.

Figure 5. Influence of the mantle lithosphere buoyancy.

The three columns correspond to the results of the three models comparing the buoyancy of the lithosphere. Organization of this figure is similar to Figure 4.

Figure 6. Comparison with the eastern Gulf of Aden.

We compare available information with the model 18 Ma after crustal break-up.

A. Comparison of the heat-flow of the model with the heat-flow profile across the northern margin [Lucazeau *et al.*, 2008]. The blue dots are heat-flow values corrected for sedimentation, topography and refraction and the green line is the modeled heat-flow.

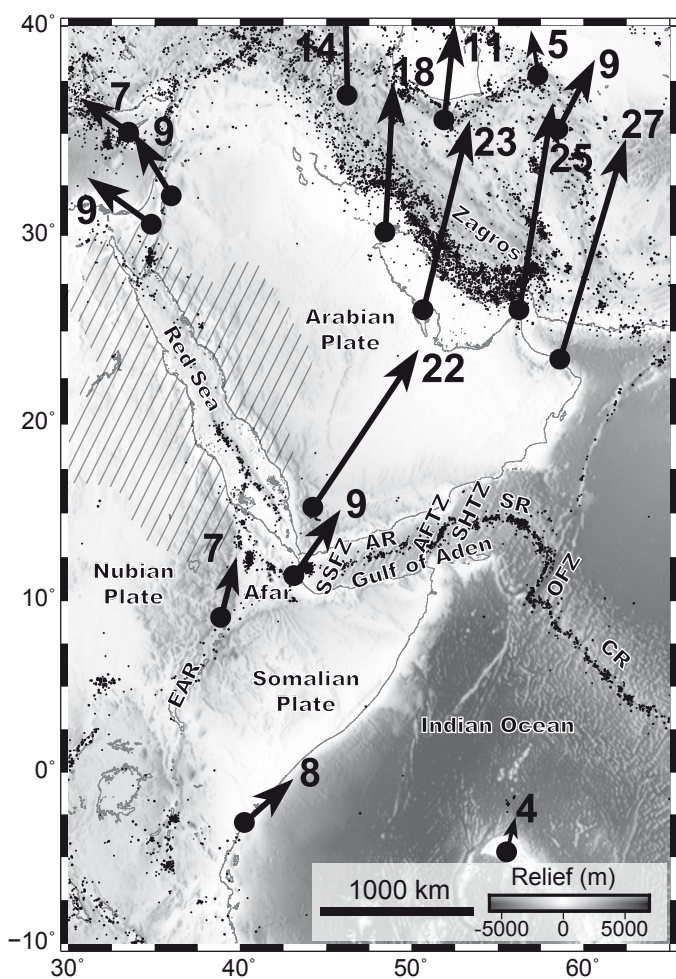
B. Comparison of the geometry of the model with a refraction and wide-angle reflection seismic profile coincident with the heat-flow measurements in part A of this figure [Leroy *et al.*, 2010a]. The grey box presents the geometry of the model and the possibility of partial melting in the mantle at the moment of crustal break-up. Z.E.C.M. means zone of exhumed continental mantle.

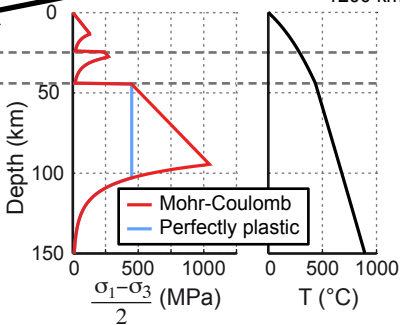
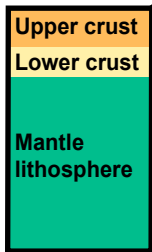
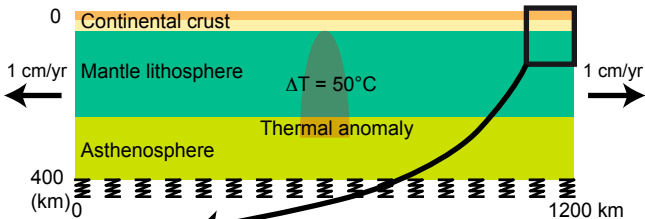
C. Comparison the model topography with data along 4 profiles [Sandwell and Smith, 1997; Farr *et al.*, 2007]. The positions of the profiles are shown on the map at the right of the figure. The red line corresponds to the position of the heat-flow/refraction line presented in A and B.

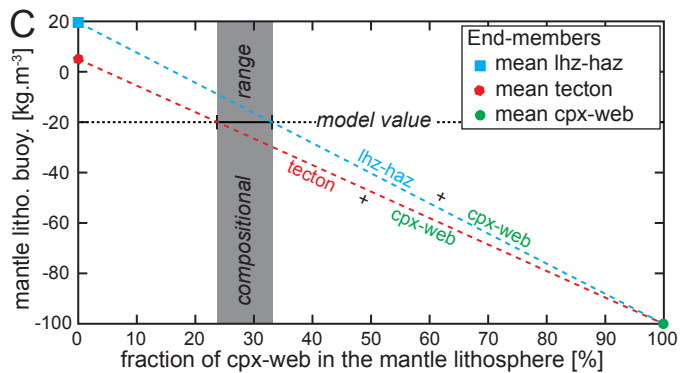
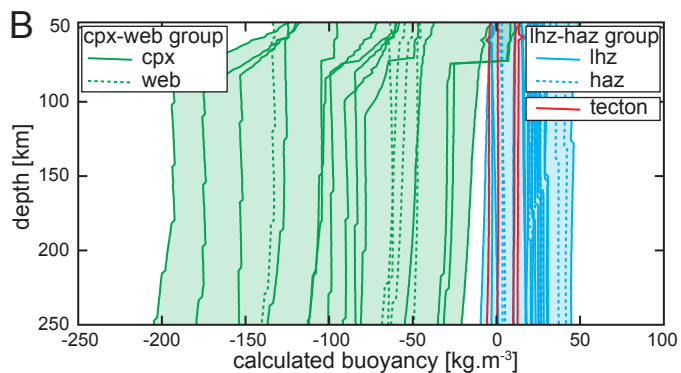
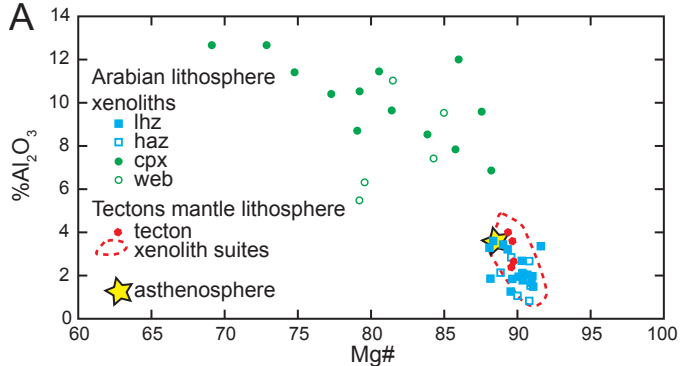
Table 1. Reference model parameters.

Parameters of the reference model having a Mohr-Coulomb failure criterion in the mantle lithosphere and equal densities in the mantle lithosphere and asthenosphere. Upper and lower crustal rheologies are dry granite and felsic granulite, respectively [Ranalli, 1995].

Parameters	Values			
Half extension velocity, V_{ext}	1×10^{-2} m yr $^{-1}$			
Temperature at the base of the lithosphere	1300 °C			
Radioactive heat production, H_s	4.5×10^{-10} W kg $^{-1}$			
Radiogenic production decay length, h_r	20 km			
Crust thermal conductivity, k_c	2.5 W K $^{-1}$ m $^{-1}$			
Mantle thermal conductivity, k_m	3.3 W K $^{-1}$ m $^{-1}$			
Specific heat, C_p	1000 J K $^{-1}$ kg $^{-1}$			
Thermal age	700 Ma			
	Upper crust	Lower crust	Mantle lithosphere	Asthenosphere
Thickness (km)	24	20	206	
Density, ρ (kg m $^{-3}$)	2750	2900	3330	3360
Initial scaling factor, A (Pa $^{-n}$ s $^{-1}$)	2.0×10^{-4}	8.0×10^{-3}	1.0×10^4	1.0×10^4
Power-law exponent, n	1.9	3.1	3.0	3.0
Activation energy, Q (J mol $^{-1}$)	137×10^3	243×10^3	520×10^3	520×10^3
Cohesion, C_0 (MPa)	20	20	20	300
Internal angle of friction, ϕ (°)	30	30	30	2
Elastic shear modulus, G (Pa)	4.4×10^{10}	4.4×10^{10}	6.7×10^{10}	7.0×10^{10}

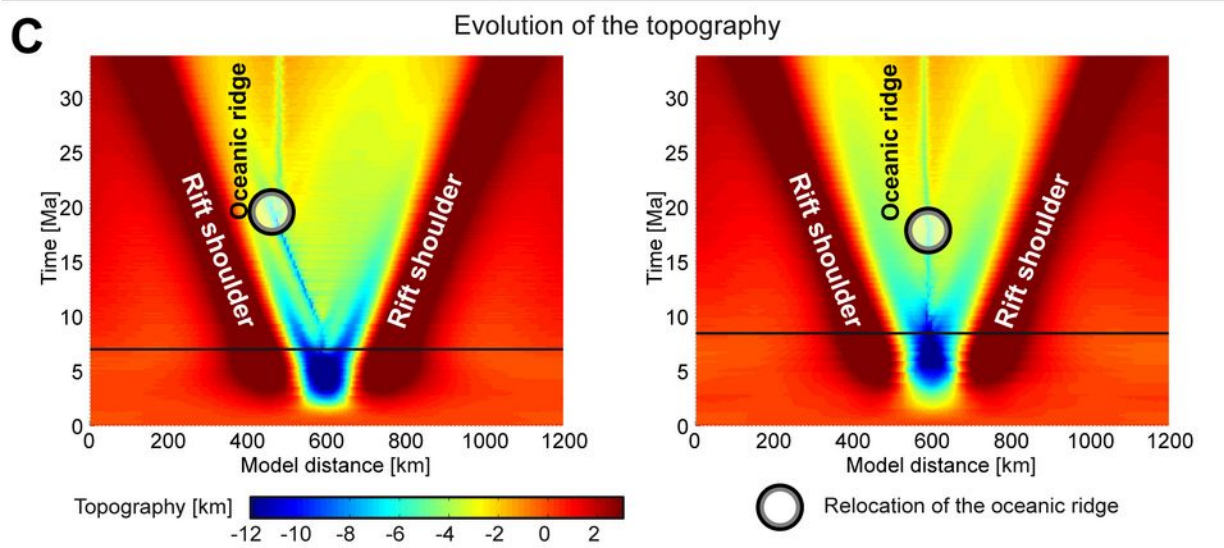
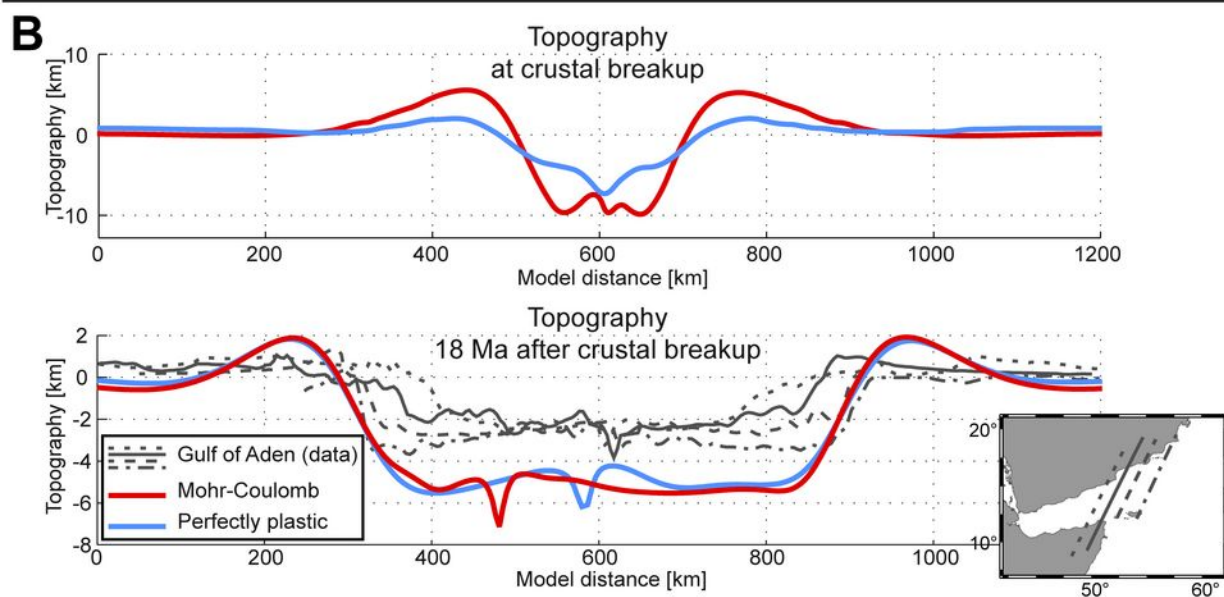
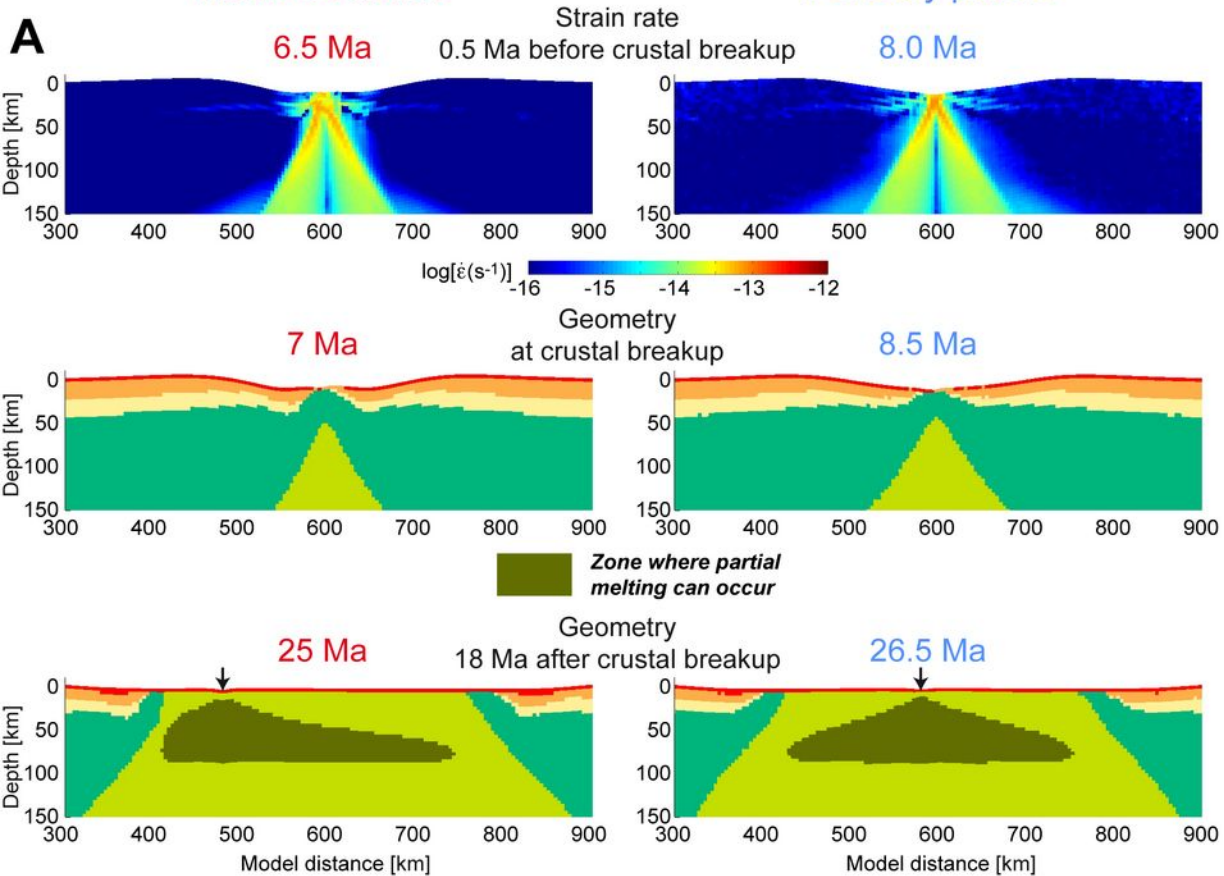


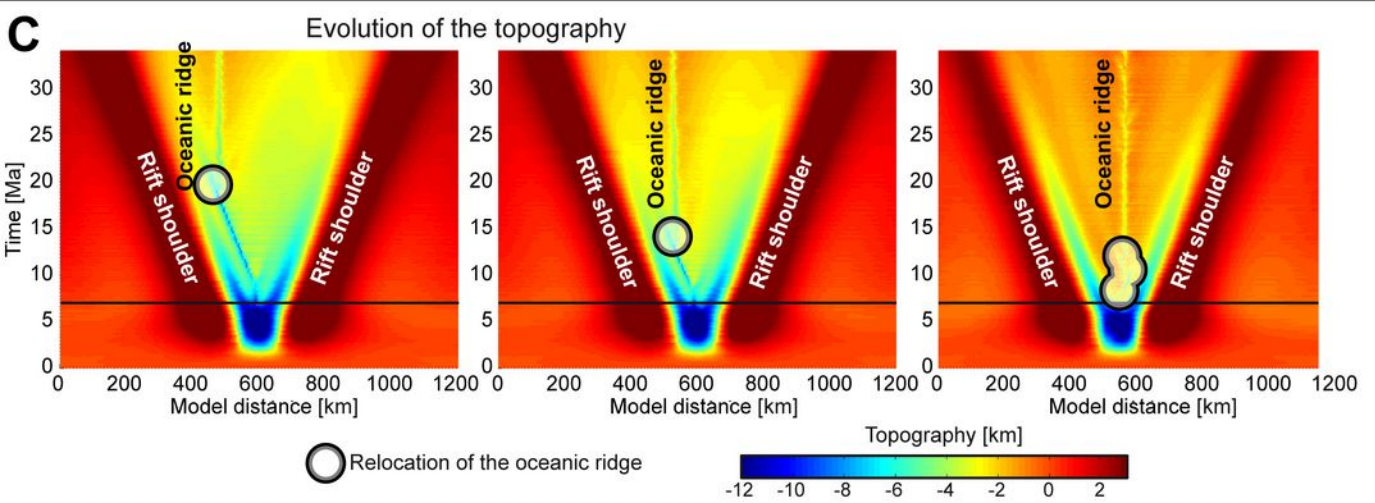
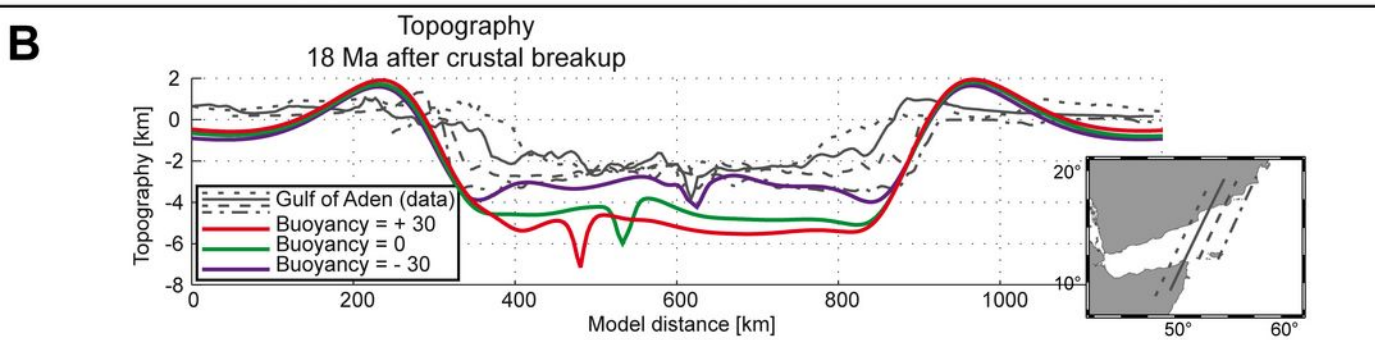
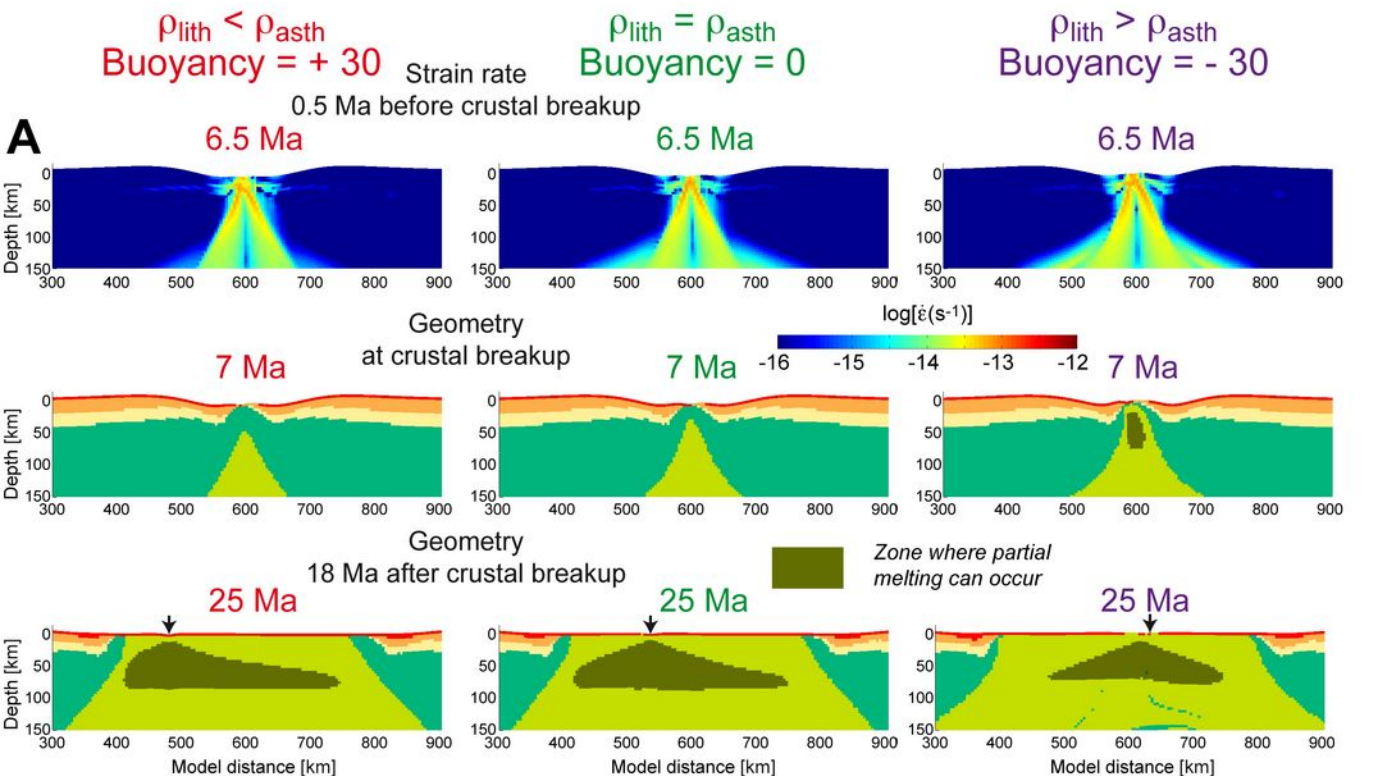


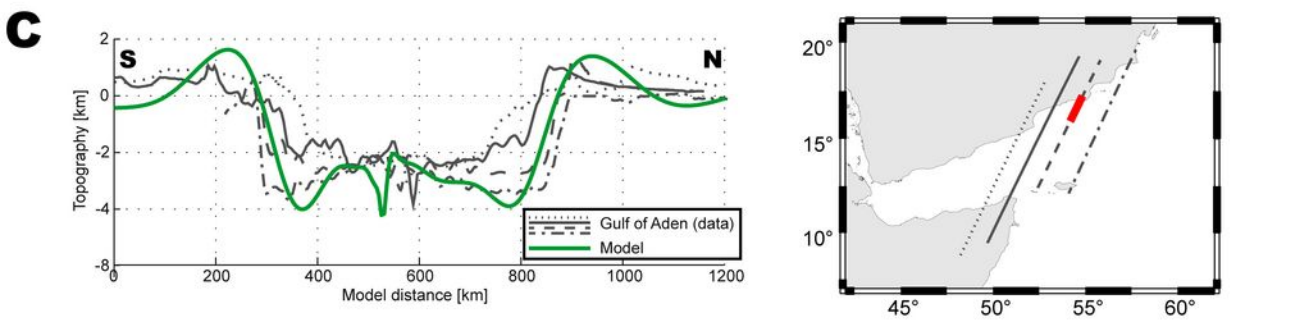
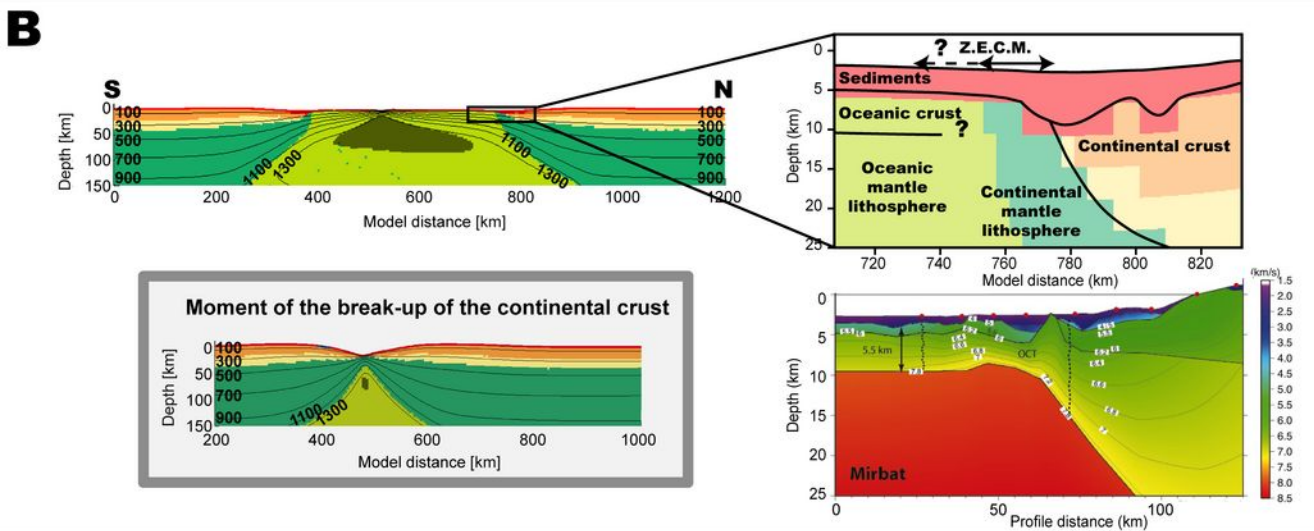
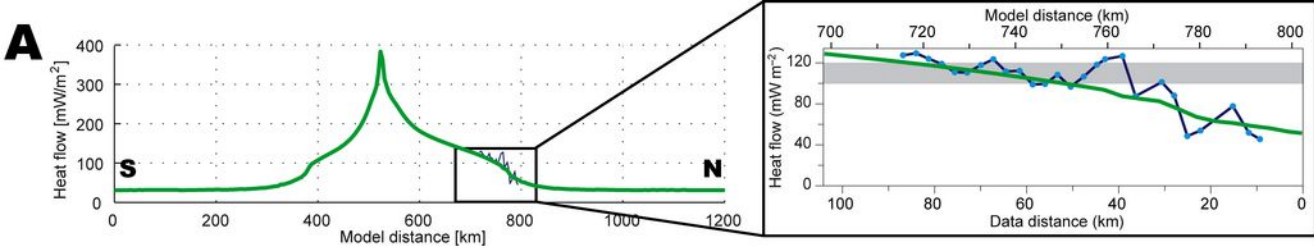


Mohr-Coulomb

Perfectly plastic







Supplementary material

1 Density of the Arabian mantle lithosphere and asthenosphere

Bulk rock chemical analyzes of xenoliths from the mantle lithosphere below the Arabian shield have been gathered from literature [*Kuo and Essene*, 1986; *Nasir and Safarjalani*, 2000; *Stein et al.*, 1993; *Ghent et al.*, 1980; *Nasir*, 1992; *Nasir and Al-Fuqha*, 1988]. These xenoliths are found in neogene alkali basalts of Yemen, Saudi Arabia, Jordan, Israel and Syria [*McGuire*, 1988]. The dataset contains analyzes of lherzolites (N=16), harzburgites (N=7), clinopyroxenites (N=13) and websterites (N=5). The analyzes of the xenoliths as well as those of the fertile Hawaiian pyrolite and of four standard compositions of mantle lithosphere below tectons (lithospheres younger than 1 Ga) are presented in table 1. The densities corresponding to these chemical analyzes have been computed with the free energy minimization program PERPLEX07 [*Connolly*, 2009]. We used a thermodynamic database that is dedicated to mantle rocks thermodynamics [*Xu et al.*, 2008]. The activity model set takes into account solid solution in plagioclase, spinel, garnet, olivine, wadsleyite, clinopyroxene, orthopyroxene and high-pressure clinopyroxene (C2/C phase) in the six oxides Na₂O-CaO-FeO-MgO-Al₂O₃-SiO₂ system (NCF-MAS). Even if the method is fairly similar, our results are not directly comparable to those of *Griffin et al.* [2009] who have not considered Na₂O in their computations. This assumption leads to higher density contrasts at depths below 400 km than with the six oxides system [*Nakagawa et al.*, 2010]. Chemical analyzes are generally given in the Na₂O-K₂O-CaO-FeO-MnO-MgO-Fe₂O₃-Al₂O₃-Cr₂O₃-TiO₂-SiO₂ eleven oxides system. Reduction from this whole system to the six oxides system has been carried out with the following assumptions. (1) The K molar amount, which is always minor, has been added to the Na molar amount. (2) The Mn molar amount, which is always minor, has been added to the Fe molar amount. (3) All iron is considered as Fe²⁺. (4) Cr and Ti are assumed to be only present as oxides (chromite Cr₂O₃ and rutile TiO₂) and are therefore not considered. Amongst all tested assumptions, this set allows us avoiding large and probably unrealistic amount of excess Al₂O₃ and SiO₂ in the clinopyroxenites and the websterites. The density with depth for all the considered chemical compositions has been computed along the initial thermal profile of the models. These curves are presented on figure 1. Following *Nakagawa et al.* [2010], only buoyancy curves rather than absolute densities are presented in the text. We indeed consider that computing density differences reduces the uncertainties unavoidably arising from the chemical analyzes, the thermodynamic database and the activity models.

Table 1: Chemical compositions of the mantle lithosphere xenoliths from the Arabian shield, tectons mantle lithosphere [Griffin et al., 2009] and asthenosphere (fertile Hawaiian pyrolite) [Wallace and Green, 1991]. The compositions are given in the reduced NCFMAS system, which has been considered for density computation with the free energy minimization program PERPLEX07 [Connolly, 2009]. Also given is the Mg# = 100 Mg/(Mg+Fe) relative to the compositions. References: 1: Ghent et al. [1980], 2: Griffin et al. [2009], 3: Kuo and Essene [1986], 4: Nasir [1992], 5: Nasir and Al-Fuqha [1988], 6: Nasir and Safarjalani [2000], 7: Stein et al. [1993], 8: Wallace and Green [1991].

Lherzolites								
Sample	M-1	K-3	T-5	A-4	R-9	JAR1	JAR3	JAR9
SiO ₂	45.92	46.06	47.16	47.02	44.66	43.44	43.72	43.03
Al ₂ O ₃	1.26	1.82	3.51	1.51	1.82	1.95	2.01	1.91
FeO	8.62	8.44	8.58	7.35	9.75	7.88	8.13	8.62
MgO	41.53	40.96	36.77	41.79	40.77	44.85	44.22	44.54
CaO	2.32	2.53	2.95	1.96	2.12	1.83	1.81	1.84
Na ₂ O	0.35	0.20	1.02	0.37	0.87	0.05	0.11	0.06
Mg#	0.90	0.90	0.88	0.91	0.88	0.91	0.91	0.90
Ref.	4	4	4	4	4	5	5	5
Sample	JAR15	JAR20	T6	B4	I1	TA-806	TA-842	MHZ-230
SiO ₂	43.62	43.39	44.70	44.69	43.01	45.16	44.69	46.81
Al ₂ O ₃	1.72	1.78	3.42	3.30	3.18	2.11	2.60	3.23
FeO	7.92	8.44	8.84	6.89	8.82	8.08	8.01	8.97
MgO	44.83	44.38	40.32	42.23	41.55	42.35	41.99	37.32
CaO	1.86	1.92	2.36	2.57	3.06	2.01	2.40	3.44
Na ₂ O	0.06	0.09	0.35	0.32	0.38	0.29	0.31	0.23
Mg#	0.91	0.90	0.89	0.92	0.89	0.90	0.90	0.88
Ref.	5	5	6	6	6	7	7	7
Harzburgites								
Sample	JT26A	JT26B	HAK-1	T3	B2	I3	H2	
SiO ₂	44.70	45.05	44.25	42.85	44.32	43.54	42.24	
Al ₂ O ₃	0.80	2.01	1.51	2.81	2.65	2.10	1.05	
FeO	8.19	8.19	7.98	9.02	7.90	9.57	9.15	
MgO	45.41	43.54	45.16	43.59	43.57	42.92	46.33	
CaO	0.80	1.01	0.92	1.46	1.40	1.70	1.17	
Na ₂ O	0.09	0.20	0.18	0.27	0.16	0.17	0.06	
Mg#	0.91	0.90	0.91	0.90	0.91	0.89	0.90	
Ref.	1	1	3	6	6	6	6	
Pyroxenites								
Sample	M-5	T-8	A-7	R-2	A-3	R-5	T1	T5
SiO ₂	54.51	53.87	53.63	52.18	51.93	51.00	44.71	46.04
Al ₂ O ₃	8.51	9.60	6.87	7.86	11.44	10.38	12.67	11.40
FeO	5.45	4.31	5.81	7.26	5.92	8.27	10.72	10.46
MgO	15.86	16.98	24.34	24.53	13.77	15.78	16.13	17.38
CaO	14.69	14.76	8.48	7.35	15.79	13.34	14.42	13.37

Continued on next page

<i>Continued from previous page</i>								
Na ₂ O	0.98	0.48	0.87	0.82	1.15	1.23	1.36	1.34
Mg#	0.84	0.88	0.88	0.86	0.81	0.77	0.73	0.75
Ref.	4	4	4	4	4	4	6	6
Sample	B7	T8	I14	BS-701	KM-1402			
SiO ₂	48.45	47.63	48.80	48.84	44.07			
Al ₂ O ₃	8.69	9.64	10.53	12.01	12.65			
FeO	8.34	7.68	9.15	4.95	11.60			
MgO	17.65	18.86	19.57	17.02	14.55			
CaO	15.24	15.30	11.16	16.07	15.92			
Na ₂ O	1.62	0.89	0.78	1.10	1.21			
Mg#	0.79	0.81	0.79	0.86	0.69			
Ref.	6	6	6	7	7			
Websterites								
Sample	58376A	58376B	58377	T15	M11			
SiO ₂	51.44	51.98	52.06	46.59	48.92			
Al ₂ O ₃	7.39	6.29	5.48	11.03	9.52			
FeO	5.90	8.94	8.61	9.68	7.53			
MgO	17.72	19.49	18.37	23.87	23.89			
CaO	16.61	12.28	14.72	8.10	8.35			
Na ₂ O	0.93	1.02	0.77	0.73	1.78			
Mg#	0.84	0.80	0.79	0.81	0.85			
Ref.	1	1	1	6	6			
Asthenosphere								
Sample	Fert-Pyr							
SiO ₂	45.80							
Al ₂ O ₃	3.59							
FeO	8.74							
MgO	38.07							
CaO	3.13							
Na ₂ O	0.67							
Mg#	0.89							
Ref.	8							
Tecton mantle lithosphere								
Sample	Tc-1	Tc-2	Tc-3	Tc-4				
SiO ₂	44.83	45.34	44.80	44.59				
Al ₂ O ₃	3.53	3.93	2.62	2.33				
FeO	8.19	8.23	8.41	8.66				
MgO	40.09	38.99	41.47	41.95				
CaO	3.12	3.22	2.52	2.23				
Na ₂ O	0.24	0.28	0.18	0.24				
Mg#	0.90	0.89	0.90	0.90				
Ref.	2	2	2	2				

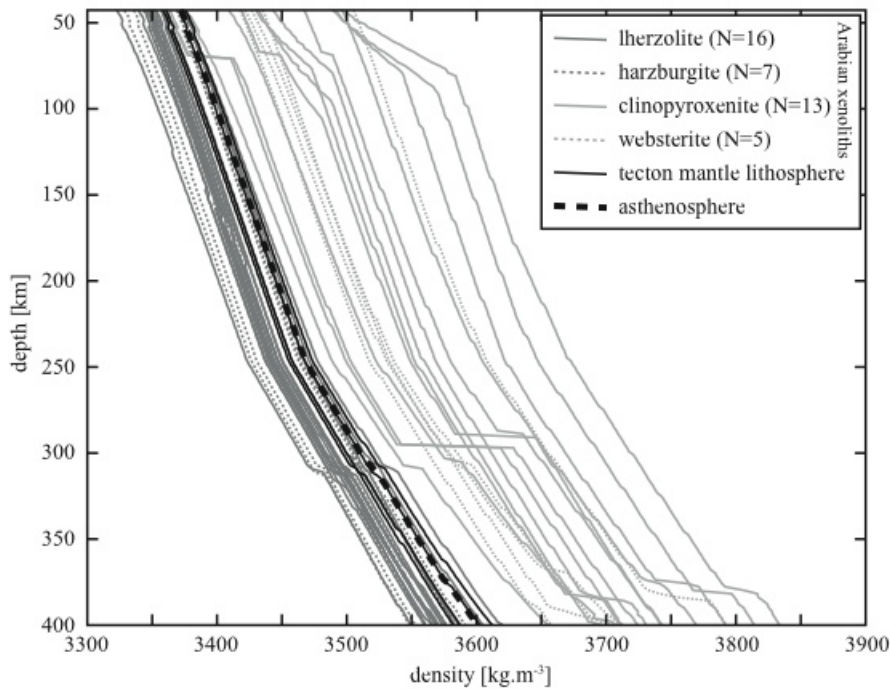


Figure 1: Density evolution with depth for mantle lithosphere xenoliths from the Arabian shield, tectons mantle lithosphere and asthenosphere. The computation of the density has been carried out with the free energy minimization program PERPLEX07 [Connolly, 2009].

References

- Connolly, J. (2009), The geodynamic equation of state: what and how, *Geochem. Geophys. Geosyst.*, 10, Q10,014.
- Ghent, E., R. Coleman, and D. Hadley (1980), Ultramafic inclusions and host alkali olivine basalts of the southern coastal plain of the Red Sea, Saudi Arabia, *Am. J. Sci.*, 280-A, 499–527.
- Griffin, W., S. O'Reilly, J. Afonso, and G. Begg (2009), The composition and evolution of lithospheric mantle: a re-evaluation and its tectonic implications, *J. Petrol.*, 50(7), 1185.
- Kuo, L., and E. Essene (1986), Petrology of spinel harzburgite xenoliths from the Kishb Plateau, Saudi Arabia, *Contrib. Mineral. Petrol.*, 93(3), 335–346.
- McGuire, A. (1988), Petrology of mantle xenoliths from Harrat al Kishb: the mantle beneath western Saudi Arabia, *J. Petrol.*, 29(1), 73.
- Nakagawa, T., P. Tackley, F. Deschamps, and J. Connolly (2010), The influence of MORB and harzburgite composition on thermo-chemical mantle convection in a 3-D spherical shell with self-consistently calculated mineral physics, *Earth Planet. Sci. Lett.*, 296(3), 403–412.
- Nasir, S. (1992), The lithosphere beneath the northwestern part of the Arabian plate (Jordan): evidence from xenoliths and geophysics, *Tectonophysics*, 201(3-4), 357–370.

- Nasir, S., and H. Al-Fuqha (1988), Spinel-lherzolite xenoliths from the Aritain volcano, NE-Jordan, *Miner. Petrol.*, *38*(2), 127–137.
- Nasir, S., and A. Safarjalani (2000), Lithospheric petrology beneath the northern part of the Arabian Plate in Syria: evidence from xenoliths in alkali basalts, *J. Afr. Earth. Sci.*, *30*(1), 149–168.
- Stein, M., Z. Garfunkel, and E. Jagoutz (1993), Chronothermometry of peridotitic and pyroxenitic xenoliths: Implications for the thermal evolution of the Arabian lithosphere, *Geochim. Cosmochim. Ac.*, *57*(6), 1325–1337.
- Wallace, M., and D. Green (1991), The effect of bulk rock composition on the stability of amphibole in the upper mantle: implications for solidus positions and mantle metasomatism, *Miner. Petrol.*, *44*(1), 1–19.
- Xu, W., C. Lithgow-Bertelloni, L. Stixrude, and J. Ritsema (2008), The effect of bulk composition and temperature on mantle seismic structure, *Earth Planet. Sci. Lett.*, *275*(1-2), 70–79.